FLEXIBLE pH SENSOR FOR SMART SENSING

by

KHENGDAULIU CHAWANG

THESIS

Submitted in partial fulfillment of the requirements

for the degree of Master of Science at

The University of Texas at Arlington

December, 2019

Arlington, Texas

Supervising Committee:

Jung-Chih Chiao, Supervising Professor

Yuze Sun

Michael Vasilyev

ACKNOWLEDGEMNTS

Completing my thesis would not have been possible without support from my supervisor, colleagues and family. I am immensely grateful to my supervisor Dr. Jung-Chih Chiao for believing in me, his confidence in me has always been a boost to explore new challenges. With his expertise and humbleness, Dr. Chiao mentored me especially during rough times in my thesis journey. Of all the days in a week, I always looked forward to the weekly meeting where we discuss on brainstorming questions. I have not only garnered academic knowledge but social skills too. I will also remember to serve society with my technical skills, kindness, and honesty; a way of life I learnt from Dr. Chiao.

I would also like to thank my colleagues from iMEMS group, Dr. Xuesong Yang whose suggestions always helped me stay on track, Shardul Pawar whose hard-working attitude has always motivated me, the kind encouragements from Dr. Souvik Dubey has been enlightening and Ethan Burt for his contribution in the experiments. My sincere thanks to staff from NanoFab UTA, Kevin and Denise who always took time to teach me tools and give insightful suggestions.

Dedication

To be able to work with some of the finest minds, in one of the finest countries, has only been possible because of my family who is my support system. Above all, my faith in Jesus Christ has been the driving force in every phase of my academic journey, I humbly rejoice the milestone achieved.

Table of contents

Acknowledgement……...i

Dedication……ii

Table of Contents…….....……...iii

List of Illustration……...vii

List of Tables……...xi

Abstract……..xii

Chapter 1 INTRODUCTION……...1

1.1 Motivation……1

1.2 Types of pH sensors……2

1.2.1 Ion Sensitive Filed Effect Transistor (ISFET) pH sensor……2

1.2.2 Fiber Optic pH sensor……...2

1.2.3 Near Infrared (NIR) Spectroscopy for pH measurement in tissue…….3

1.2.4 Metal Oxide pH sensor…….3

Chapter 2 IRIDIUM OXIDE BASED SENSOR BY DIP COATING METHOD……4

2.1 Fabrication steps……..4

2.2 Study on types of Sol-Gel based pH sensor……7

2.2.1 Sensitivity……7

2.2.2 Hysteresis……9

2.2.2.1 Size of the electrode……...10

2.2.2.2 Effect of initiation point……14

2.2.3 Response time……15

2.2.4 Repeatability……..17

2.2.5 Interference test……..19

2.3 Sol-Gel based sodium sensor…….23

2.4 Working of Commercial reference electrode…….24

2.5 Discussion……..25

Chapter 3 IRIDIUM OXIDE BASED PH SENSOR BY ELECTROPLATING METHOD……27

3.1 Fabrication process…….27

3.1.1 Solution preparation……...27

3.1.2 Sample preparation and instruments used……..28

3.2 Cyclic Voltammetry (CV) plot and sensor performance……29

3.2.1 Chromium based samples……...29

3.2.2 Copper based samples……31

3.2.2.1 Samples prepared in NanoFab, UTA……..31

3.2.2.2 Dupont samples……..33

3.3 Discussion……..34

Chapter 4 DEVICE PACKAGING……35

4.1 Packaging process……..35

4.2 Approach to develop sensing window……36

4.2.1 Laser Cutter……37

4.2.2 Surgical blade…….38

4.2.3 Position of window…….39

4.2.4 Punch plier……40

4.3 Response time study……..41

4.4 Skin test……43

4.5 Discussion……..44

Chapter 5 LAMINATED SENSOR ARRAY……....45

5.1 Objective……45

5.2 Sensor fabrication……..46

5.3 Results……47

5.3.1 Sodium sensor……48

5.3.2 pH sensor……51

5.3.2.1 Hydration problem……51

5.3.2.2 Size of sensing window……52

5.3.2.3 Insulation problem or electrode design……..53

5.3.2.4 Sample contamination……54

5.3.2.4.1 Hysteresis and Sensitivity study part I……55

5.3.2.4.2 Hysteresis and Sensitivity study part II……...57

5.3.2.5 Trouble shoot……59

Chapter 6 PH VALUE DISPLAY……61

6.1 Materials and tool used……..61

6.2 pH value display on digital screen……62

6.3 Concept for wireless pH sensing……63

Reference……...64

Bibliographical information……..….65

List of illustration

Figure-1. Cross sectional view of three samples fabrication step……5

Figure-2. Gold film difference in type I, II and III samples after dip coating……..6

Figure-3. Cured copper-based samples (type II and III)……6

Figure-4. Sensitivity plot tested for three days……8

Figure-5. Sensitivity plot restricting size of the electrode……8

Figure-6. Demonstration of hysteresis calculation……10

Figure-7. Hysteresis and precision plot of type I electrode with and without DI wash……11

Figure-8. Hysteresis and precision plot of type II electrode with and without DI wash……12

Figure-9. Hysteresis and precision plot of type III electrode with and without DI wash……13

Figure-10. Hysteresis plot based on initiation point……15

Figure-11. Demonstration on how response time data is identified……16

Figure-12. Response time based on electrode size and metal type……16

Figure-13. Demonstration on how repeatability data is identified……17

Figure-14. Repeatability plot at pH 4,7 and 10, for 20 cycles……18

Figure-15. Repeatability plot at pH 4,7 and 10, for 40 cycles……18

Figure-16. Type I. (a), (b) and (c) plots at fixed pH with varying salt concentration. (d) Sensitivity plot at different salt (NaCl) concentration……..19

Figure-17. Type II at fixed salt concentration, pH variation……...20

Figure-18. Type II at fixed pH, salt concentration variation……..21

Figure-19. Type III at fixed salt concentration, pH variation…….21

Figure-20. Type III at fixed pH, salt concentration variation……..22

Figure-21. Interference test of type I, II and III in different salt concentration……..22

Figure-22. Molecular structure and sodium ion captured by B12C4…….24

Figure-23. Cross sectional view of an Iridium Oxide based Sodium sensor……...24

Figure-24. Silver chloride commercial reference electrode……25

Figure-25. Solution color before (a) and after (b) four days……28

Figure-26. Type I CV plots (a) 100 cycles (b) 150 cycles (c) 200 cycles (d) 250 cycles……29

Figure-27. Type I hysteresis plot at 100, 150, 200 and 250 cycles…….30

Figure-28. Type I sensitivity plot tested for 6 days deposited with different number of sweeps/cycles…….30

Figure-29. CV plot for copper-based samples (type II and III) under 150 and 200 cycles……31

Figure-30. Hysteresis and Sensitivity plot of samples (II and III) with 150 and 200 cycles……..32

Figure-31. (a) Cracked copper-based samples (b) Au layer peeling off during sensitivity tests…..32

Figure-32. Dupont sample CV plot for (a) 50 cycles, (b) 80 cycles and (c) 100 cycles…….33

Figure-33. Dupont samples (a) hysteresis plot and (b) high voltage range……34

Figure-34. Design flow of device packaging. (a) laminating pouch, (b) double tape, (c) window punctured out using biopsy punch, (d) Data acquisition from a laminated sample…….36

Figure-35. Real time current reading by NI DAQ card……...37

Figure-36. Sample with rough edges using laser cutter……..38

Figure-37. (a) crocodile clippers wrapped in copper foil (b) Laminated sample using surgical blade……...38

Figure-38. Sensitivity and response time plot…….39

Figure-39. Position of sensing window……..39

Figure-40. Sensitivity and response time plot of (a)Window in the middle (b) Window in the corner…….40

Figure-41. Sensitivity and response time of punch plier samples……..41

Figure-42. Demonstration how laminated samples are tested in presence of magnetic stirrer…..41

Figure-43. Saturation time study, by running 2 cycle hysteresis tests, with DI wash……..42

Figure-44. Sensitivity and response time study……..42

Figure-45. Skin test set up……..43

Figure-46. Hysteresis study for skin test at buffer pH 4, 7 and 10……..43

Figure-47: Sensitivity plot tested at buffer pH 4, 7 and 10…….44

Figure-48. Sensor array……..47

Figure-49. Crosstalk test between working electrodes……...48

Figure-50. Uncalibrated data……..49

Figure-51. Calibrated data……..49

Figure-52. Hysteresis plot of sodium sensing channel……50

Figure-53. Sensitivity plot of sodium sensing channel……...50

Figure-54. A flexible and ultra-flexible electrode tested in artificial sweat……51

Figure-55. Film peeling image when tested for 4 cycles (eight hours)……52

Figure-56. Effect of window size on sensor performance……..53

Figure-57. Improper insulation……...53

Figure-58. Hysteresis study of sensor array with proper insulation……54

Figure-59. (a) Sample in plasma chamber (b) tool information……54

Figure-60. Hysteresis and sensitivity plot before lamination, before plasma treatment……55

Figure-61. Hysteresis and sensitivity plot after lamination, before plasma treatment……56

Figure-62. Hysteresis and sensitivity plot after lamination, after plasma treatment……56

Figure-63. Buffer and A.S at pH 5,6,7 and 8 under condition one……..57

Figure-64. Buffer and A.S at pH 5,6,7 and 8 under condition two……..58

Figure-65. Buffer and A.S at pH 5,6,7 and 8 under condition three……58

Figure-66. Two electrode design……59

Figure-67. Tools used for pH value display……61

Figure-68. Differential amplifier circuit……62

Figure-69. Real time pH value display……...63

List of Tables

Table-1. Sample types with different metal layers……4

Table-2. Category of electrodes for different tests……9

Table-3. Repeatability data for 20 and 40 cycles……17

Table-4. Material information……35

Table-5. Trials in developing sensing window using laser cutter……37

ABSTRACT

FLEXIBLE PH SENSOR FOR SMART SENSING

Khengdauliu Chawang, Master of Science

The University of Texas at Arlington, 2019

Supervising Professor: Jung-Chih Chiao

pH level of biofluid is crucial in understanding physiological health. Commercial glass electrode pH sensors are bulky and cannot provide real time data. In this study, a novel miniature pH sensor capable of continuous wireless communication was developed, which is a promising technology for providing point-of-care diagnosis. Iridium Oxide because of its wide pH sensing range and biocompatibility has attracted attention from biomedical and food industries; high sensitivity of Iridium Oxide based sensor is attributed to its high charge density. Flexible polyamide Kapton substrate (127 µm) is taken as base substrate and E-Beam method is employed to deposit adhesion and metal layers. Electrodeposition processes such as Electroplating and Sol-Gel methods are employed to deposit Iridium Oxide on the Gold (Au) film. Electroplated electrodes showed high sensitivity (Super Nernstian response) and shorter lifetime, where-as Sol-Gel electrodes showed good sensitivity (Nernstian response) with longer lifetime. Hysteresis study based on the adhesion layer showed that Chromium (Cr) based samples exhibited higher hysteresis over Copper (Cu) based samples. But a combination layer of Cu over Cr, layered under the Au film showed the best performance. This type of samples was studied to attain super Nernstian response with sensitivity of about 62mV/pH and low hysteresis among other electrode types. Further, device packaging with cost effective and method to display pH reading on digital screen using Arduino (a low power consumption tool) is also reported.

Chapter 1

INTRODUCTION

1.1 Motivation

pH value is an important indicator to study acidic or alkaline level of any aqueous solution. It is expressed as negative logarithmic of ionic hydrogen concentration and obeys the Nernst equation. pH value scales from 0 to 14, 7 is neutral, acidic nature corresponds to pH value lower than 7 and alkaline nature corresponds to values above 7. Their respective natures become extreme as they move away from neutral value of 7. With growing technology, realization of pH sensor is becoming an interest in biomedical, food and cosmetic industries. Traditionally, a litmus paper was used as a pH indicator. In the early 20'th century, research on pH sensor became ubiquitous industrially and academically. This led to development of glass-based pH sensor, which has thrived for long in the market due to their longevity and stability. However, a litmus paper cannot provide precise pH reading, and glass-based pH sensors are bulky and incapable of providing continuous data. These limitations make them inapt for pH monitoring in biomedical and food industries. Glass-based pH sensor are currently used to study skin pH for people suffering from medical skin conditions. Such clinical approaches are unreliable and stressful for the patients. Therefore, a miniature and flexible pH sensor that is biocompatible and allows real time data acquisition will ease arduous clinical procedures.

For health status, analytes in the biofluids can provide important biomarkers, glucose sensing from sweat being one of the most successful so far [1]. Tissue health is also reported to be directly related to pH level. Integrating pH sensor and RF device on a chip can allow wireless

communication that provides real time data. Such a technology is also promising in *in vivo* study and will also boost our understanding of food borne diseases during global food supply chain.

1.2 Types of pH sensors

Advancement in healthcare over the early 20th century has pushed boundaries for the need to recognize role of pH sensors in understanding physiological health. The ability to continuously track pH level of food provides real time information on freshness or spoilage of food. Some of the earliest pH sensing devices [2] are discussed here.

1.2.1 Ion Sensitive Field Effect Transistor (ISFET) pH sensor

ISFET pH sensor is type of early potentiometric pH sensor where Silver Chloride (AgCl) works as the reference electrode (RE) and a glass electrode sensor as the reference electrode. The working principle is based on the potential difference between the working and reference electrode like a basic transistor where ions from the solution creates a field between the source and drain. Commercially, the product is encapsulated inside a glass tube and has been used in the Biomedical industries but due to their bulky size and challenges in miniaturization or conformability it is not applicable for *in Vivo* application.

1.2.2 Fiber optic pH sensor

Light transmitted through the optical fiber probes the sensor to measures hydronium ion concentration. For long monitoring gastric acid reflux has been a critical, such a type of sensor allows *in vivo* monitoring of acidity in the gastro-esophagus with sensing range of pH 1 to pH 8. When high accuracy of ionic strength is not of concern this is a sensor that upbeats most other categories since there is a lesser chance of Electromagnetic interference, safer for *in vivo* application due to alternative use of light as source rather than current through the probe. Although

shrinking has been possible, yet the brittleness of the sensor still is a challenge and therefore is not applicable for biomedical applications where conformability is of high interest.

1.2.3 Near Infrared (NIR) Spectroscopy for pH measurement in tissue

Need for patient comfort while physiological health monitoring is of high interest clinically, NIR Spectroscopy is a non-invasive tool which works on the principle that pH level of protein present in the tissue changes the absorption spectrum. To implement such a tool calls for complicated unportable system and thus, though it fulfills the need of non-invasive wireless monitoring yet fails to meet miniaturization requirement.

1.2.4 Metal Oxide pH sensor

Most solid-state pH sensors developed cannot meet the need for miniaturization and mass production. Metal oxides such as Iridium oxide (IrO_2), platinum oxide (PtO_2) and titanium Oxide (TiO_2) have been studied to meet the requirements, however they do suffer from potential fluctuation and hysteresis [refer]. Among types of metal Oxides, Iridium Oxide stands out to be the most promising candidate in biomedical and food industries; owing to its biocompatibility and ease in fabrication processes. Research claims on working principle of the material is attributed to the redox reaction that occurs, sensitivity is dependent on the oxidation state of the film. Thin film can be prepared by thermal oxidation, Electrochemical (Sol-Gel and Electroplating) and Sputtering processes. Iridium oxide film grown electrochemically have been studied to have good sensitivity attaining Nernstian response of 59 mV/pH. Sputtering process is not an economical fabrication process, due to expensive target cost it becomes incompatible for cost effectiveness. With these factors in mind, this research has focused on developing Iridium Oxide sensors, electrochemically grown on a flexible polyamide substrate, ensuring biocompatibility and cost effectiveness.

Chapter 2

IRIDIUM OXIDE BASED PH SENSOR BY DIP-COATING METHOD

2.1 Fabrication steps

Three types of electrodes are prepared, based on adhesion layer, which is deposited on flexible Kapton polyamide substrate. Parameters such as sensitivity, hysteresis, response time and potential fluctuation has been studied. Metal layers for all three types of electrodes have been prepared using E-Beam deposition tools available in the NanoFab, UT Arlington cleanroom. Adhesion layers such as Cr and Cu have been deposited using CHA Electron-Beam Evaporator tool, Au layer is deposited using the tool AJA ATC Orion Series Thermal Evaporator. The deposition rate of Cr, Cu and Au is monitored at 0.1 Aº/S, 0.2 Aº/S and 0.2 Aº/S respectively.

Dip-coating is a very simple type of fabrication process which does not include using sophisticated tools or tough fabrication process. Solution is prepared by first mixing a gram of anhydrous Iridium Chloride ($IrCl_4$) in 42 ml of ethanol, after stirring them well in a beaker, 10 ml of acetic acid (80%) is added. To properly mix the solution, a magnetic stirrer is used which is rotated at 500 RPM, and beaker is placed on the stirrer for two hours. For best results, solution is left undisturbed for about a week at 4ºC.

Type	Number of metal layers	Adhesion layer	Metal layer (Top to bottom) thickness
I	2	Chromium (Cr)	Au (200 nm) + Cr (50 nm)
II	2	Copper (Cu)	Au(200nm) + Copper (50nm)
III	3	Chromium (Cr)	Au (200nm) + Cu (50nm) + Cr (30nm)

Table 1 – Samples types with different metal layers

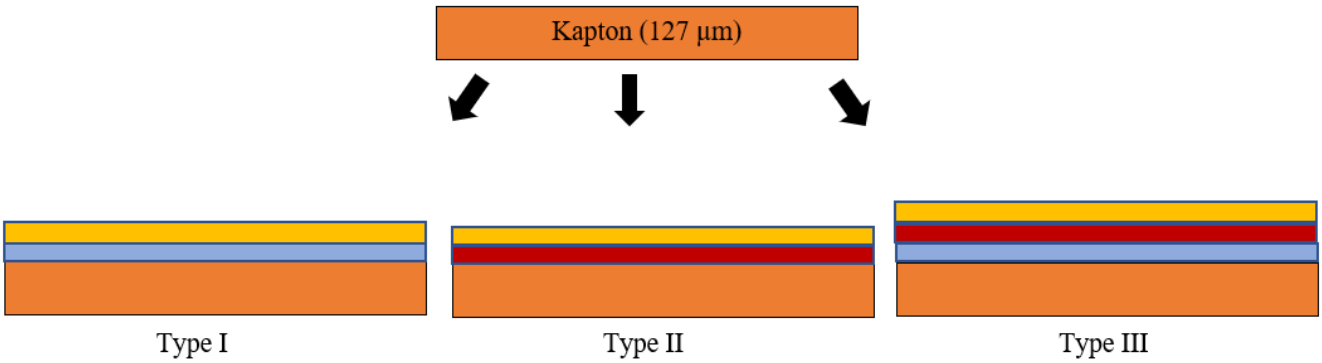

Fig 1 – Cross sectional view of three samples fabrication step

There are basically five steps involved in depositing iridium oxide (IrOx) film namely emersion, start-up, deposition, drainage and evaporation. Depositing IrOx film on type I sample is relatively a mature Sol-Gel process, the recipe can be obtained from number of articles. To ensure film uniformity and thicker film, all samples are dip coated 3 times, with 10 minutes air dry interval before every consecutive dip coating. After air drying the samples, they are introduced for annealing on hot plate. After every one-hour temperature is increased, samples are annealed first at 25°C, then up to 125ºC and further to 225º. After this, plate temperature is increased to 325ºC, and samples are further heated for four more hours. The annealing process overall takes 7 hours.

The chemical reaction involved in the oxidation process at temperature of 300ºC is:

$$2IrCl_4 + 3H_2O \longrightarrow Ir_2O_3 + 6HCl + Cl_2 \quad (1)$$

Preparation of type II and type III samples are a modified process of type I sample. The use of Cu as one of the metal layers created severe cracks on Au film. Degradation in film quality was not expected during the drying process at room temperature. To tackle this problem, we hypothesized a situation: evaporation or drying process is long enough for acidic Sol-Gel solution to seep through the metal layers and lift it off. Thereby, leading to cracked and uneven surfaces. Samples II and III were dried on the hot plate at 50ºC for few seconds to expedite evaporation process,

allowing the gold film to stay intact. This procedure solved the problem and provided a smoother IrOx film after sample preparation (see figure 3) even when treated at high temperature.

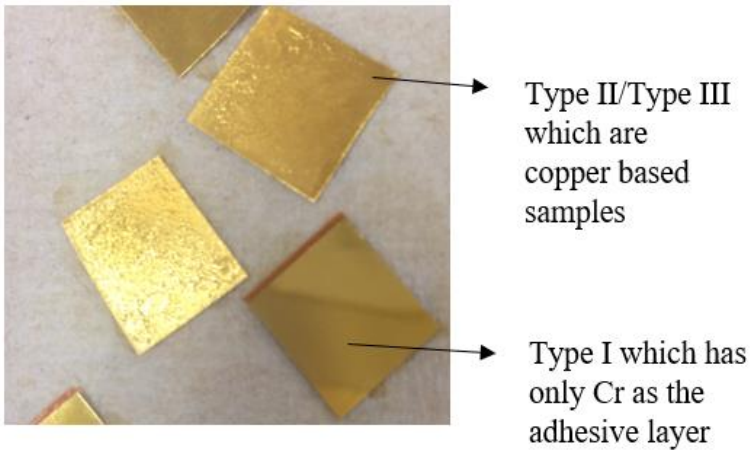

Fig 2 – Gold film differences in type I, II and III samples after dip coating

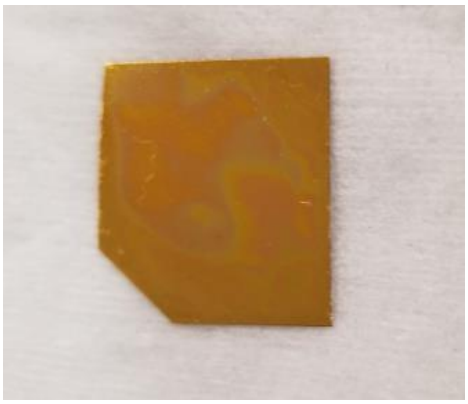

Fig 3- Cured copper based samples(type II and III)

Fabrication process of type II and type III samples.

a. Dip coat sample in Sol-Gel solution.
b. Place sample on hot plate for 10-15 seconds heated at 50ºC.
c. Repeat step 1 and 2 for 2 more times to ensure better film.

d. Allow sample to dry on hot plate set at 25ºC for an hour. After an hour each, increase the temperature to 125ºC and further to 225ºC, and finally to 325ºC for four hours. The overall heating process takes 7 hours.
e. Turn off the hotplate and let samples cool down, also further let it rest for 12 hours at room temperature.

In the following studies, most samples show near Nernstian response, Nernstian response or super Nernstian response. Such a behavior can be explained due to the presence of hydrogen ion activity and the chemical reaction is:

$$Ir_2O_3 + 6H^+ + 6e^- \longleftrightarrow 2Ir + 3\,H_2O \quad (2)$$

$$IrO_2 + 4H^+ + 4e^- \longleftrightarrow Ir + 2H_2O \quad (3)$$

$$2IrO_2 + 2H^+ + 2e^- \longleftrightarrow Ir_2O_3 + H_2O \quad (4)$$

After dip coating the samples with Iridium Oxide film, they are made to rest at room temperature for 12 hours, samples are cut into strips of different sizes (1x10 mm^2, 2x10 mm^2, 3x10 mm^2) and copper wires are attached to the stripped samples using silver epoxy. For better conductivity, silver epoxy is used glue wire and samples, and left to dry for 12 hours again.

2.2 Study on types of Sol-Gel based pH sensor

2.2.1 Sensitivity

Batch of five electrodes, for all three electrode types like discussed in part 2.1 are prepared. To study electrode sensitivity, buffer solution of pH levels 1,4,7,10 and 13 are used as testing solutions.

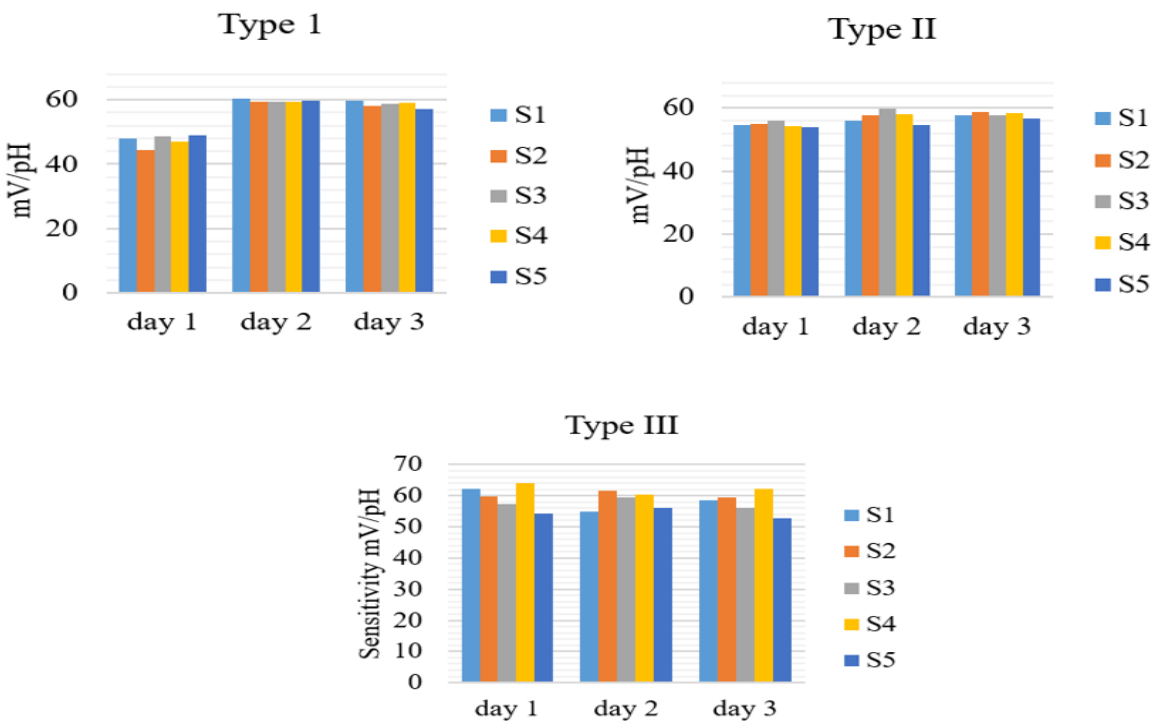

Fig 4 – Sensitivity plot tested for three days.

Electrodes were tested for 3 days in the same pH range; type II electrodes showed a consistent performance since day 1 and all electrodes has a wide sensing range.

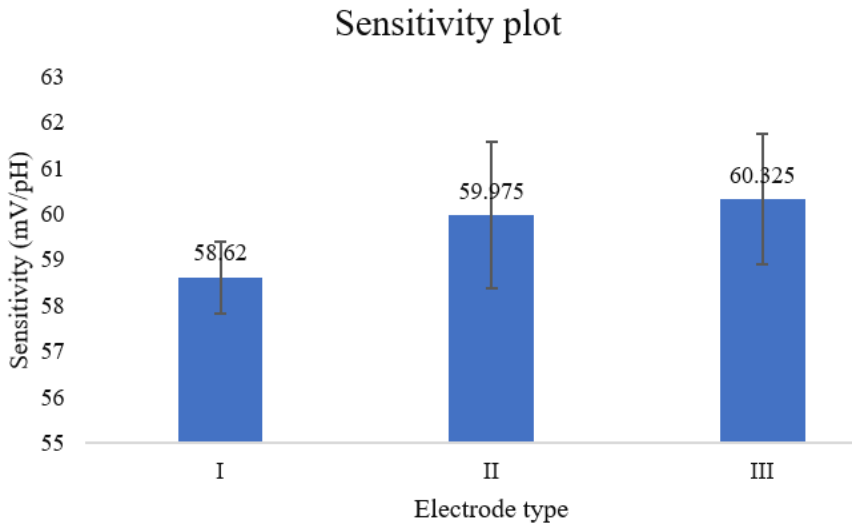

Fig 5- Sensitivity plot restricting size of the electrode.

Another sensitivity test was carried out by preparing 5 electrodes each for all three types of electrodes and restricting size of the electrodes to 1x10 mm^2. Combination of two metal layers in type III electrodes were found to exhibit highest sensitivity. Chromium (Cr) and Copper (Cu) are materials with good adhesivity and conductivity, and their combination in type III enhances sensor performance.

2.2.2 Hysteresis

From research data, hysteresis is known to exist in electrodes prepared by electrochemical process. Research by dash group states that hysteresis can be affected by factors such as electrode size and initiation point. To understand the influence of these factors on hysteresis behavior, this part of the research focused on intensively studying their effects. For study on size influence, 45 electrodes in total were prepared, 15 electrodes for each type, categorized into size 1, size 2 and size 3. For Initiation point, tests are performed at buffer solution under two conditions: starting at buffer pH 1 and going to pH 13 and starting at buffer pH 13 and going to pH 1.

Category for hysteresis study based on		Type I	Type II	Type III
Size	Size 1 (1x10 mm^2)	5	5	5
	Size 2 (2x10 mm^2)	5	5	5
	Size 3 (3x10 mm^2)	5	5	5
Initiation point		5	5	5

Table 6- Category of electrodes for different tests.

2.2.2.1 Size of the electrode

Effect of size on hysteresis was studied, electrodes are also tested on condition with and without DI (Deionized) water wash. Data plots of ΔV vs pH and ΔpH vs pH is plotted for understanding hysteresis effect and electrode precision. Tested from pH 1 to pH 13 and vice versa, hysteresis value is calculated by averaging the steadied data, and subtracting the two data set between each pH level.

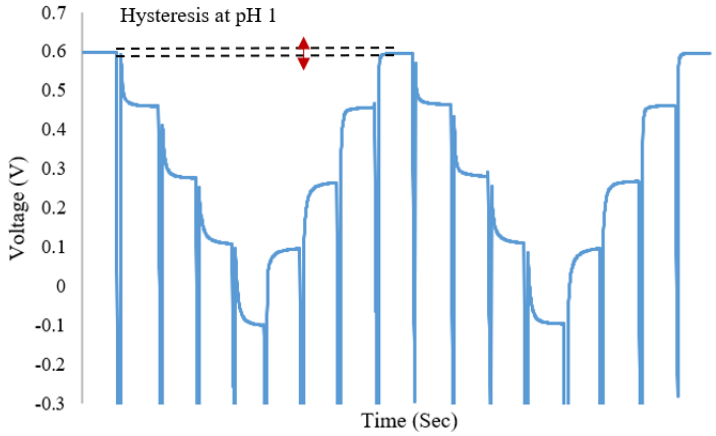

Fig 6 – Demonstration of hysteresis calculation

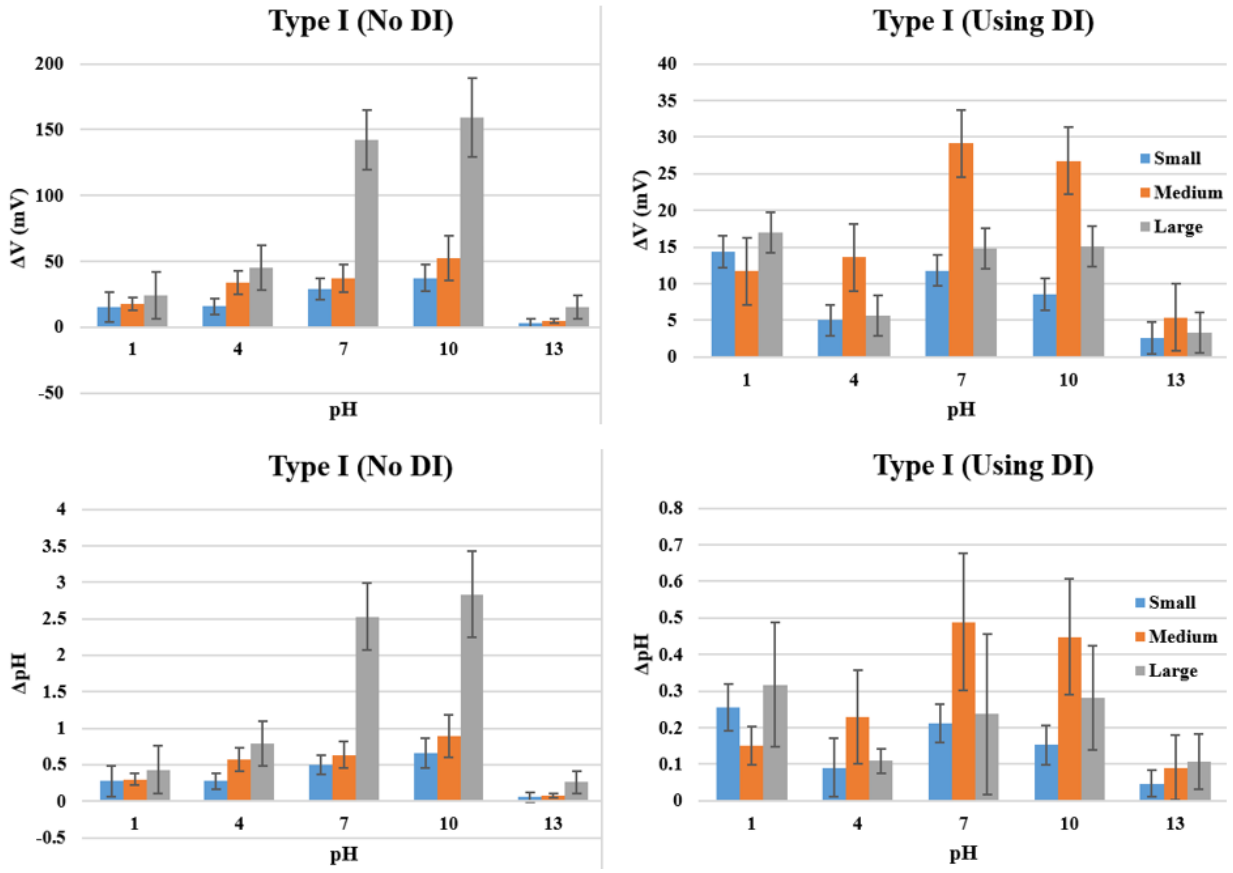

Fig 7 – Hysteresis and precision plot for Type I electrode with and without DI wash

From fig [], type I electrode is analyzed to suffer from severe hysteresis when electrode is not washed in water, but hysteresis decreases by 60mV with when electrodes are washed in DI water. Size 3 electrode (3x10 mm^2) with largest sensing area (3x2 mm^2) suffers from severe hysteresis. Without wash treatment, size 3 has highest hysteresis at pH 10 of 180mV. Size 1 electrode has comparatively lower hysteresis than size 2 and size 3 all pH levels.

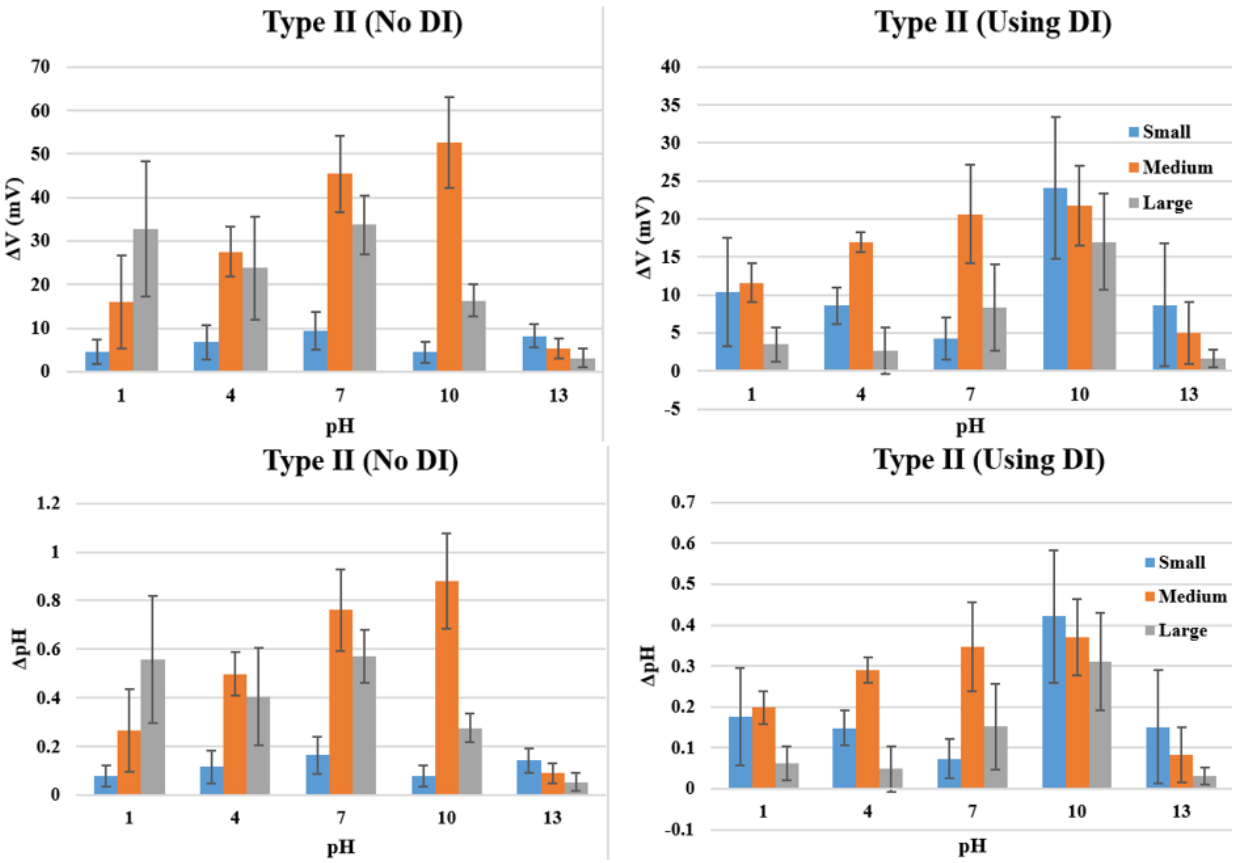

Fig 8 – Hysteresis and precision plot for Type II electrode with and without DI wash

From fig 8, it can be analyzed that hysteresis and precision are lowest for smaller electrode size, with higher hysteresis in the neutral range. In a condition where there is no DI wash, type II and type III electrodes showed lesser hysteresis and higher precision than type I electrodes. Size of the electrodes effect hysteresis performance.

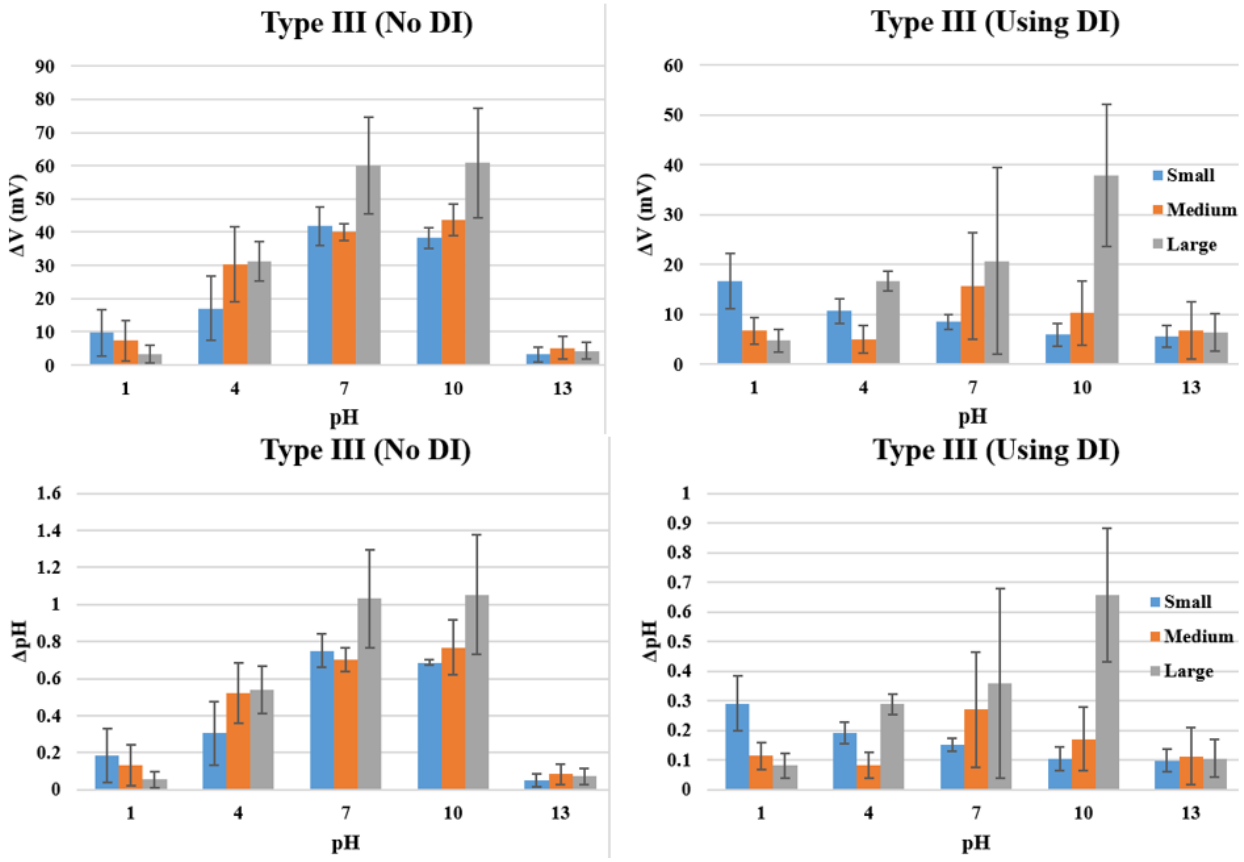

Fig 9 – Hysteresis and precision plot for Type III electrode with and without DI wash

Analyzing the plotted data of hysteresis effect, it can be understood that smaller size has lowest hysteresis for all the three electrode types. Hysteresis is also contributed by surface roughness that traps residue in the porous film. Washing the electrodes in DI water removes residue by washing away ions, and thereby reduces hysteresis effect. To understand natural environment where DI wash is not always possible like invasive or minimally invasive environments, it is important to observe data without DI wash also.

A precision plot for ΔpH vs pH allows us to understand how precise pH reading will be at each pH level. Among all electrode types, large size of type I electrode has lowest precision but under

DI wash it attains similar precision like type II and type III electrodes. Precision number is also becomes severe in the neutral range for all electrode types.

By comparison, type I electrodes highest hysteresis of about 190 mV but under DI wash decreases to about 35 mV. Highest hysteresis observed in type II electrode is about 60 mV but under DI wash decreases to 30 mV. Type III electrodes shows highest hysteresis of about 70 mV and with DI wash decreases to about 45 mV. Chromium (Cr) is a material with high impedance which creates lesser current and this creates larger potential difference, contributing to high hysteresis effect. Type I and III has Cr as one of the metal layers which explains why they have higher hysteresis. Copper (Cu) on the other hand is a material with high conductivity, allowing high current which creates lesser potential difference. Type II has copper as one of the metal layer which allows higher conductivity and helps in improving hysteresis performance.

For situations, when electrodes cannot be washed in DI water, type II and type III performs better than type I. An observation common in all three electrode types of different sizes is that neutral range has highest hysteresis and lowest hysteresis is observed at extreme acidic (pH 1) and alkaline (pH 13) levels. Smaller electrode size (1x10 mm^2) has smaller sensing area (1x2 mm^2), having to lose lesser number of hydroxyl groups which are responsible for hysteresis; common behavior in all three types of electrodes. From this study based on size of electrodes, size 1 (1x10mm^2) showed least hysteresis.

2.2.2.2 Effect of initiation point

To study the worst-case scenario, size of electrode has been restricted to large size (3x10 mm^2) with sensing area of about (3x1 mm^2). From the plotted data we can analyze that samples with copper as one of the metal layers (type II and type III) exhibits lower hysteresis compared to type

I; with highest hysteresis when initiation point is at alkaline level. Type I electrode exhibits higher hysteresis when initiation point is from acidic level except at pH7 they have similar hysteresis effect. All three electrodes have higher hysteresis in the neutral range. An interesting observation is that every type of electrode has lowest hysteresis in extreme acidic or alkaline buffer solution; similar behavior is also observed with effect of size on hysteresis study.

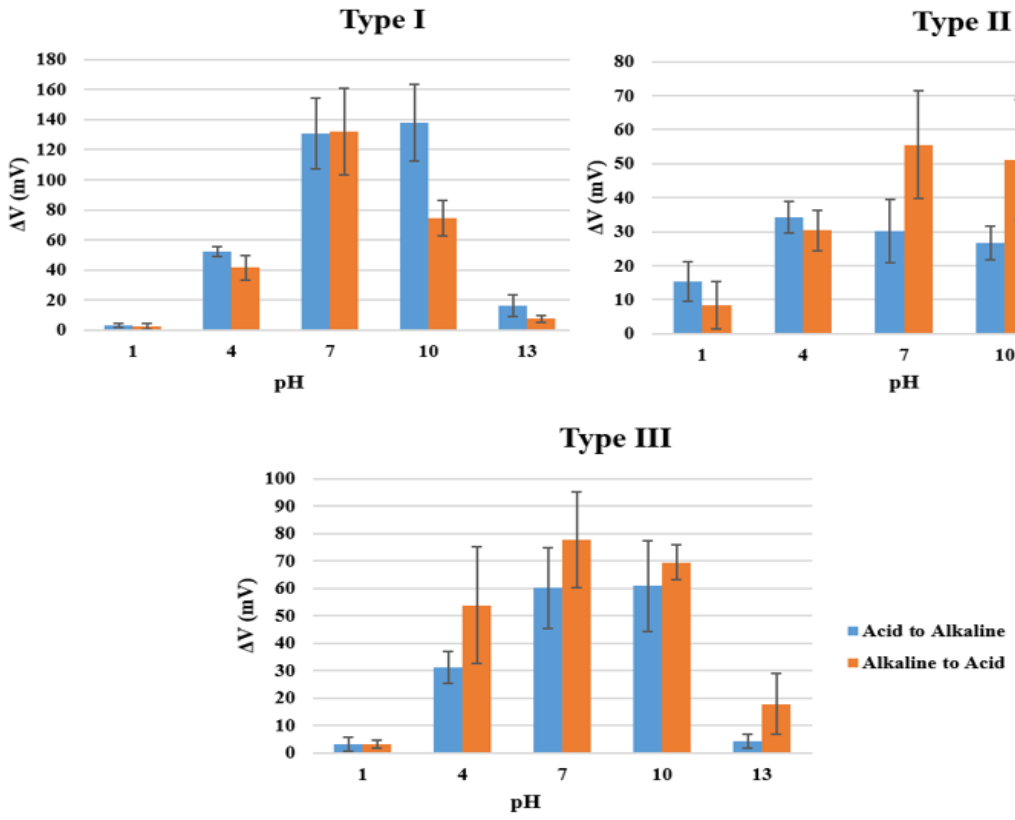

Fig 10 – Hysteresis plot based on initiation point

2.2.3 Response time (can you use resistivity formula to explain this?)

According to Huang et al [3], response time is defined as the time needed for the sensor to reach a stable potential (value that is 90% of the saturated value) and a stable sensitivity is achieved thereafter. Below is a figure of how a typical response time value is identified.

Regardless of sample type, from Fig 10 smallest electrode size samples has the fastest response time. This indicates faster response of such electrodes in less than 6 seconds even at pH of 7. All three types and sizes of electrodes show stable response in about 6 seconds.

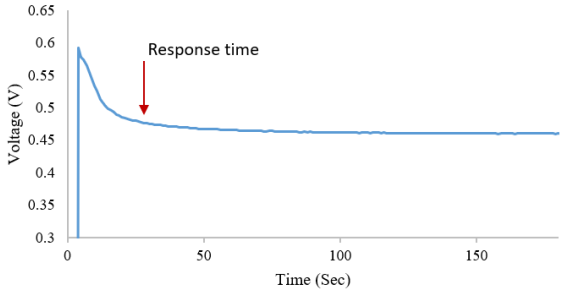

Fig 11 - Demonstration on how response time data is identified

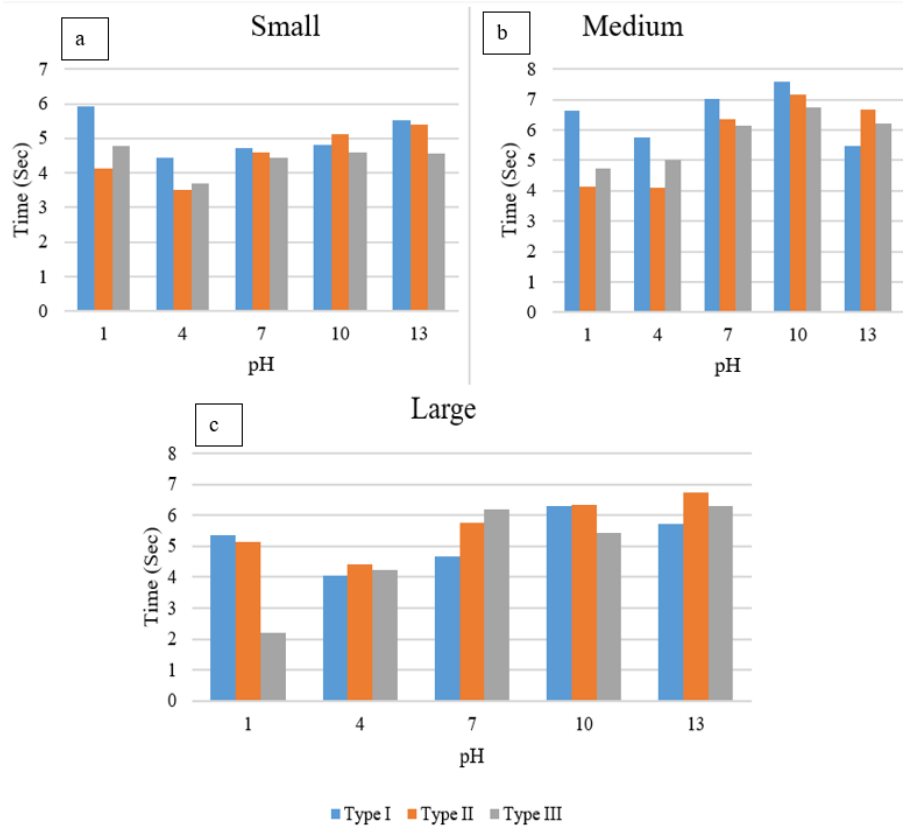

Fig 12 – Response time based on electrode size and metal type

2.2.4 Repeatability

The experiment is carried out to know the stability of the sensor, if same voltage is generated even after repeated or multiple use. Each data point is collected after the potential has stabilized. Testing solution is pH 4,7 and 10. To see if sensor performance is repeatable, the cycle is repeated 20 to 40 times and difference between the maxima and minima value are calculated at each pH level.

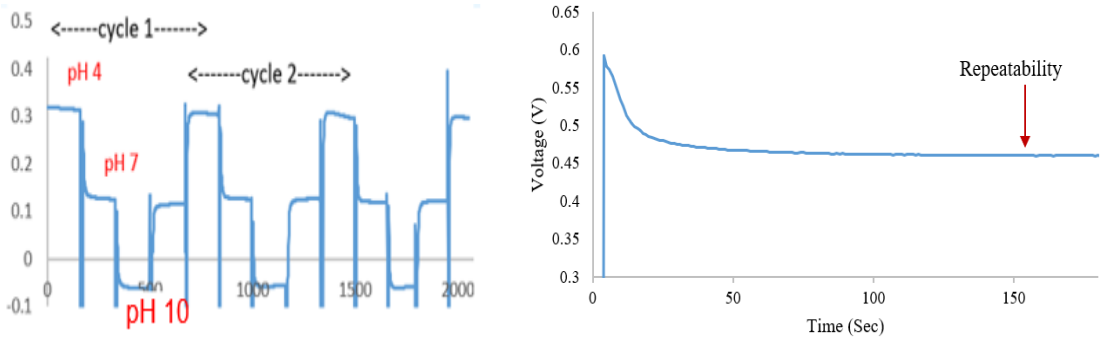

Fig 13 - Demonstration on how repeatability data is identified

	20 cycles			40 Cycles		
Type	I	II	III	I	II	III
4	21.2	44.2	101.7	41.7	84.6	70
7	24.3	29.7	57.6	21.9	50.6	41.7
10	17.1	26.6	33.9	13.4	34.5	28

Table 3- Repeatability data for 20 and 40 cycles.

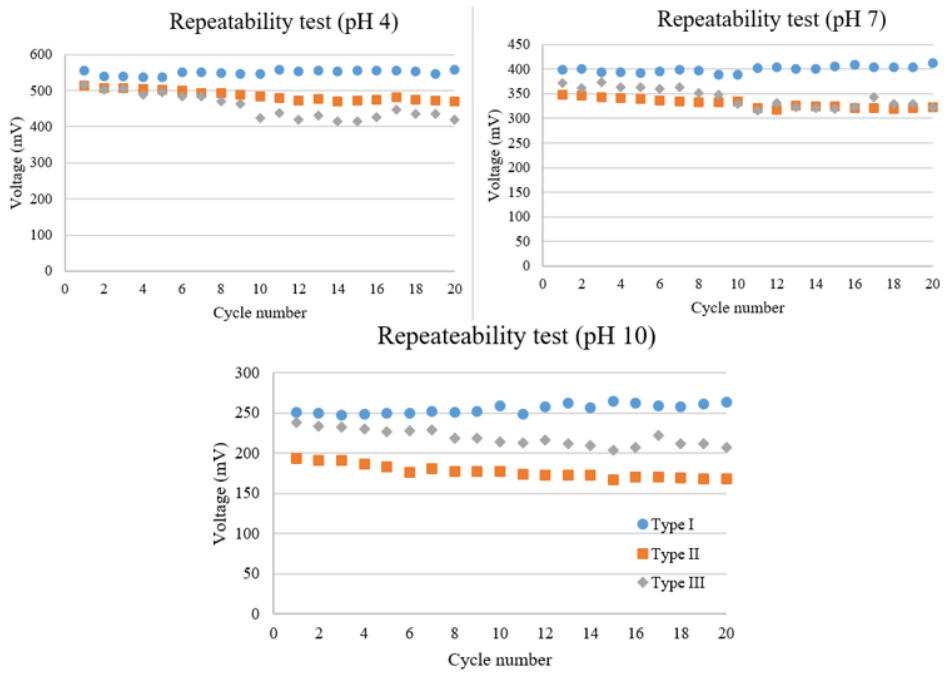

Fig 14 – Repeatability plot at pH 4, 7 and 10 for 20 cycles.

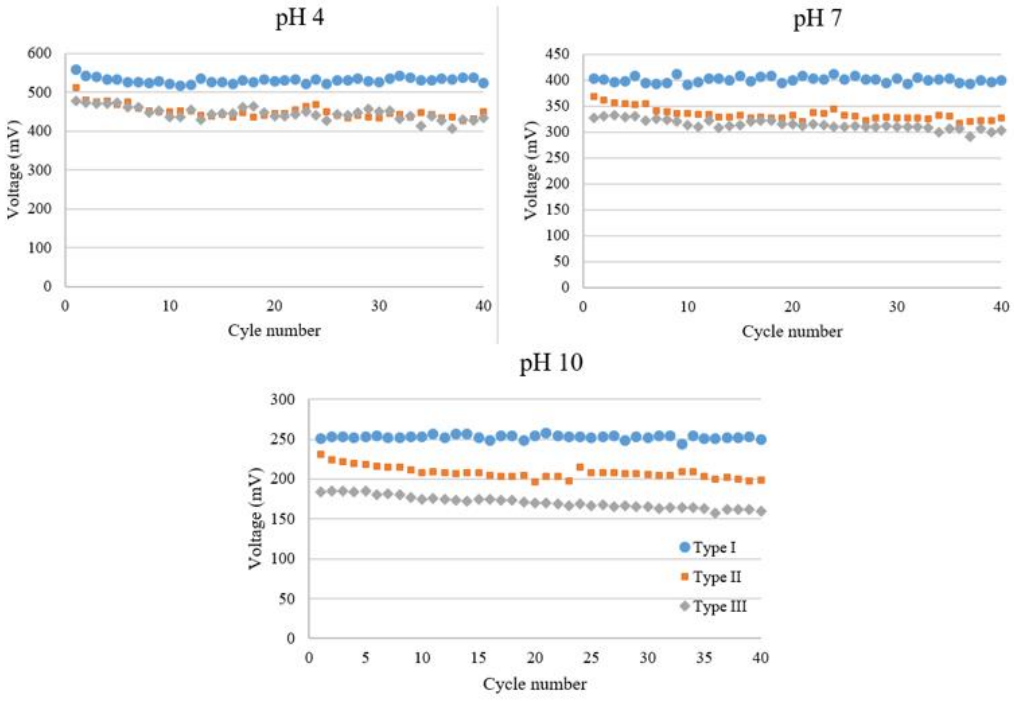

Fig 15 - Repeatability plot at pH 4,7 and 10 for 40 cycles

Fig 14 and 15 is a plot of 20 and 40 cycles tests done from pH 4-7-10 and vice versa, data is plotted for all three types of electrodes. Type II and III samples, which has copper as one of the metal layers, generates closer potentials at every respective pH levels. Type I sample has best repeatability with lowest potential difference generated than other two types.

2.2.5 Interference test

pH value depends on hydronium ion concentration, and presence of salts such as sodium and potassium are common in biological related environments. To understand influence of these ions on pH reading is crucial. Overlooking such interferences will provide abnormal readings, causing greater problems when precise reading is the goal.

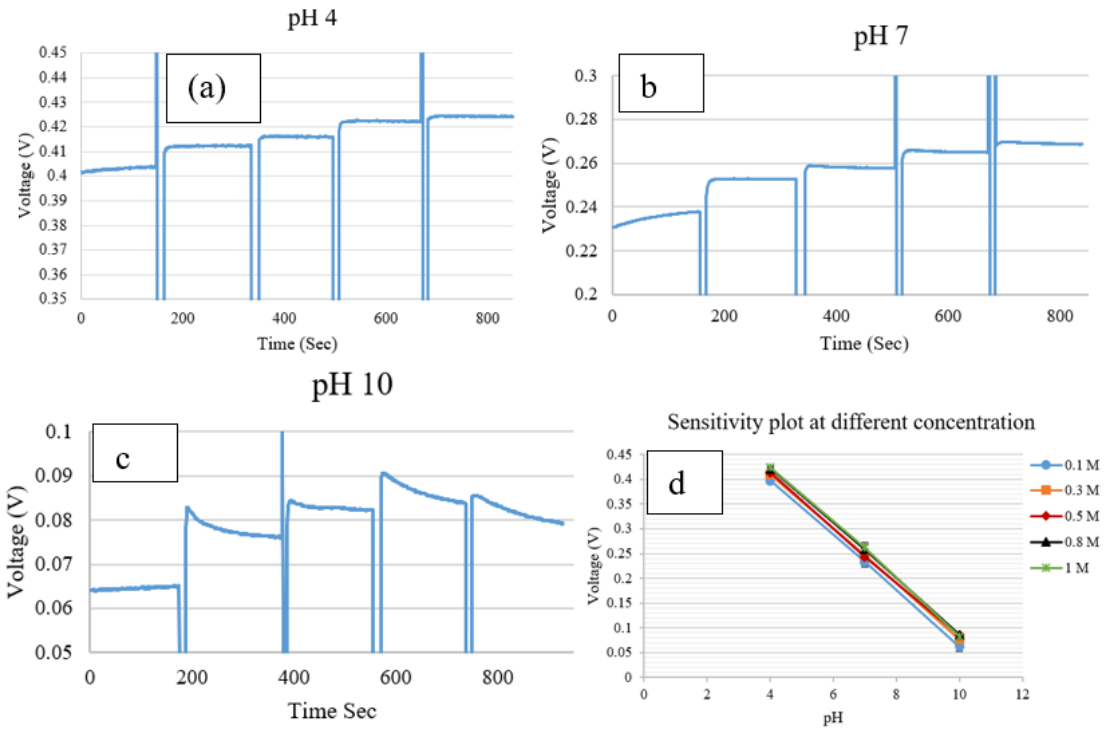

Fig 16 – Type I. (a), (b) and (c) plots at fixed pH with varying salt concentration. (d) Sensitivity plot at different salt (Nacl) concentration.

Interference test on type I samples has been done on a batch of 5 sensors, it is carried out by increasing salt concentration while the pH remains same. From Fig-d it can be perceived that though there is an influence on potential contributed by higher salt concentration, yet sensitivity of the sensor remains unchanged.

After observation that presence of salt can be detected by pH sensor, we moved on to Two types of interference tests were experimented: one at fixed pH with variation in sodium chloride salt (Nacl) concentration, other where salt concentration is fixed with variation in pH levels of the solution.

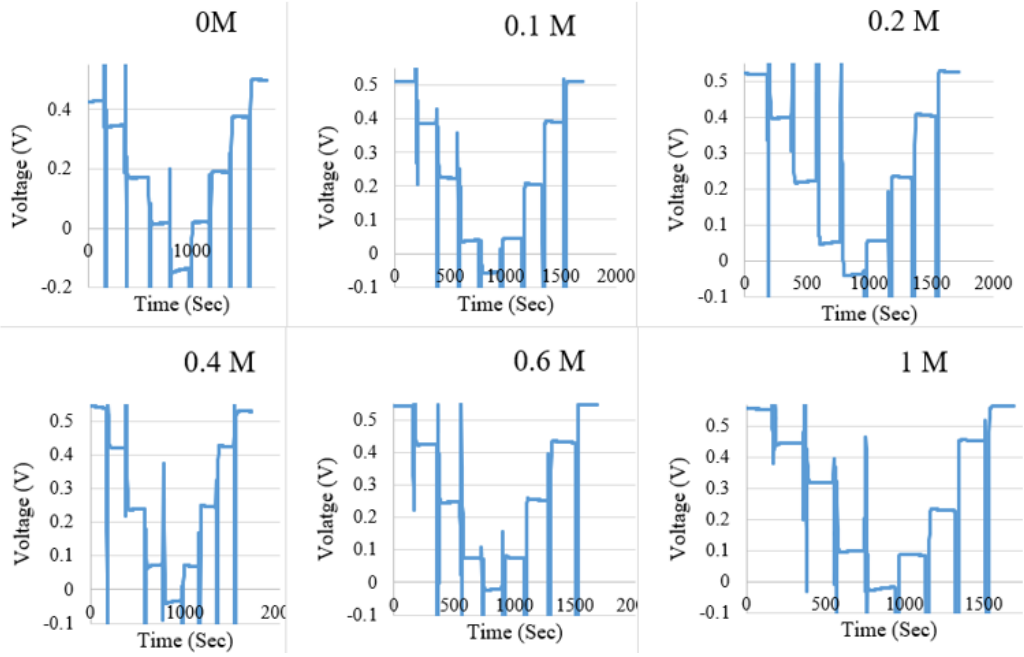

Fig 17 – Type II at fixed salt concentration, pH variation

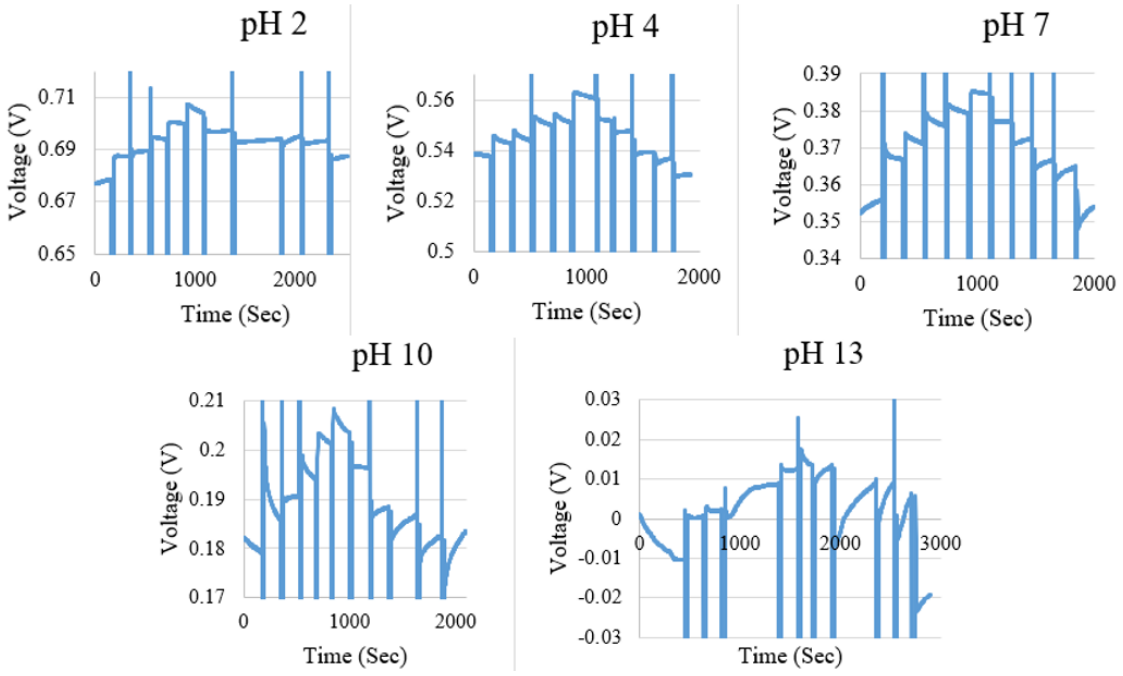

Fig 18 – Type II at fixed pH, salt concentration variation

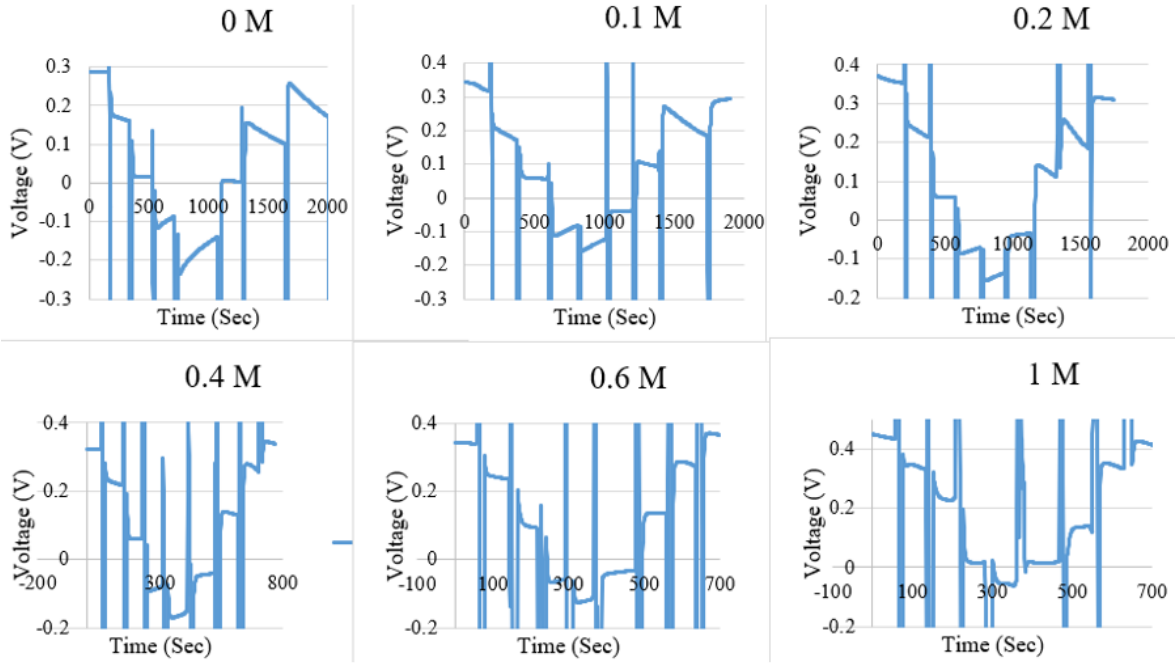

Fig 19 – Type III plots at fixed salt concentration, pH variation.

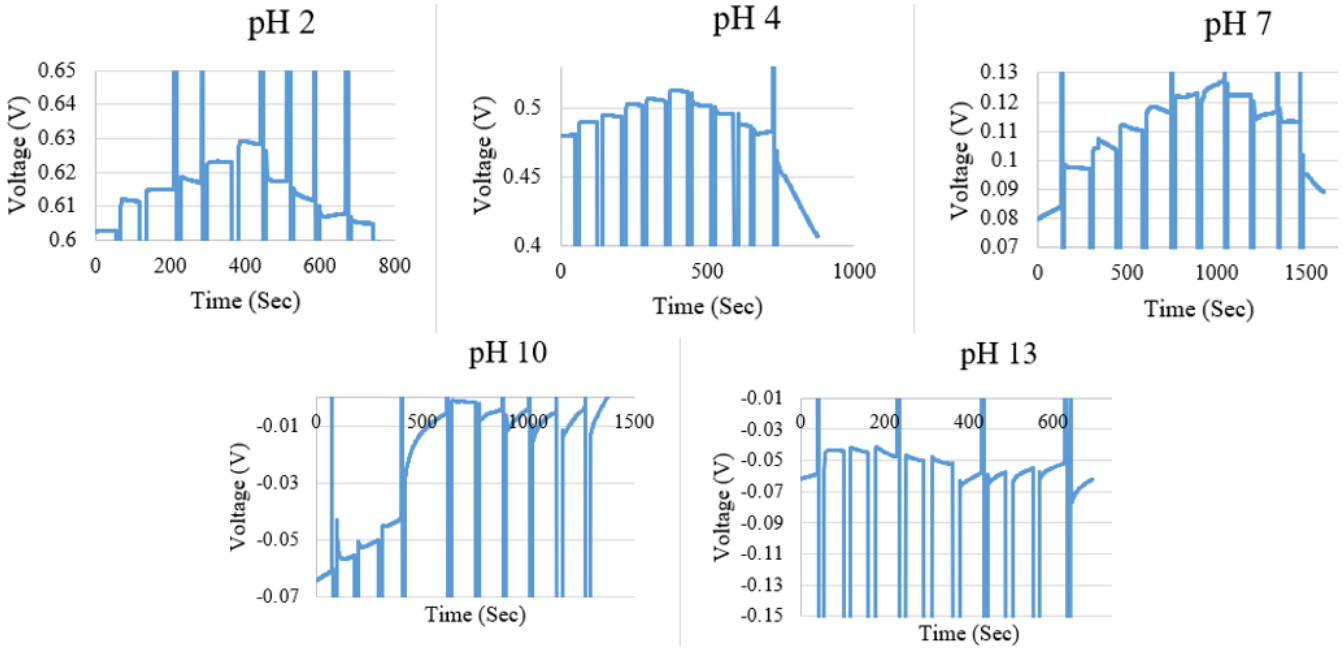

Fig 20 – Type III at fixed pH, salt concentration variation.

Comparing plots at fix pH concentration with varying salt concentration; the electrode type II and III detects change in salt concentration in acidic medium but not in high alkaline medium. And regardless of medium, severe hysteresis is also common in three electrode types. In the experiment (fig), when salt concentration is fixed and pH level is changed, type II electrode has best response. Type II electrode has lesser hysteresis over type I and type III.

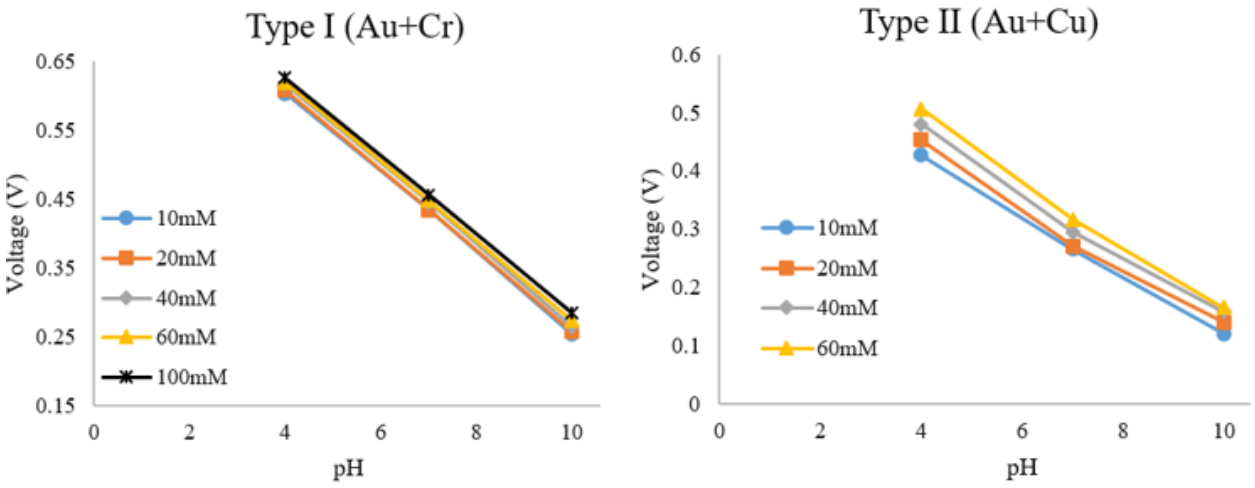

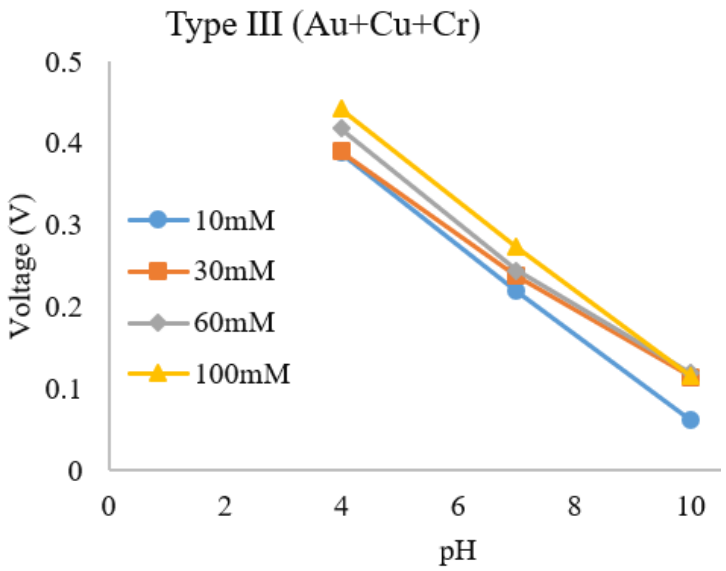

Fig 21- Interference test of type I, II and III in different salt concentration.

From fig 21, it is clear that electrodes detect change in salt level without compromising sensor performance. Type I, II and III has a step response of 9mV, 26mV and 27mV.

2.3 Sol-Gel based Sodium sensor

Sodium ion exists predominantly in the extracellular fluid and is an essential electrolyte in maintaining the pH and electrolyte balance in the human body. Excess of sodium ions can lead to health disorders such as high blood pressure, but it can be tackled with proper dietary, however an abnormally low amount of sodium ion can lead to life threatening problems such as hyponatremia. Therefore, proper monitoring of sodium ion is important, this chapter of research focuses on creating a flexible Iridium Oxide based electrode for sodium sensing. A variety of crown ethers are used for sodium sensing or alkali metal detection, here solid-state electrode using PVC is employed and sodium ionophore VI (B12C4) is the active component int sodium ion sensing.

Materials needed to prepare a sodium ion sensing film were purchased from Sigma, the recipe is:

a. 550 mg of poly carboxylate (PVC-COOH) mixed with 8 ml of tetrahydrofuran is left in the Ultrasonicator 30 minutes for proper mixing.

b. Next a 1.2 ml of bis (2-ethylhexyl) sebacate (DOS) is mixed and left for more 10 minutes.

c. Finally, 50 mg of sodium ionophore V1(B12C4) and 167 mg lipophilic salt (Na-TFBD) are mixed and left further for 30 minutes more.

d. The viscous mixture is then applied onto the pre-prepared iridium oxide samples, they are left at room temperature to rest for 24 hours.

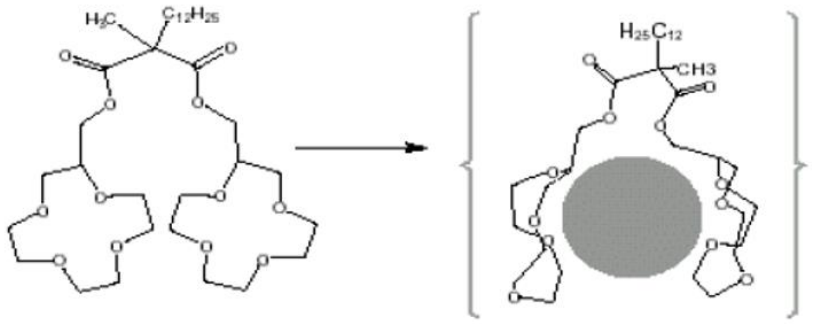

Fig 22 – Molecular structure and sodium ion capture by B12C4

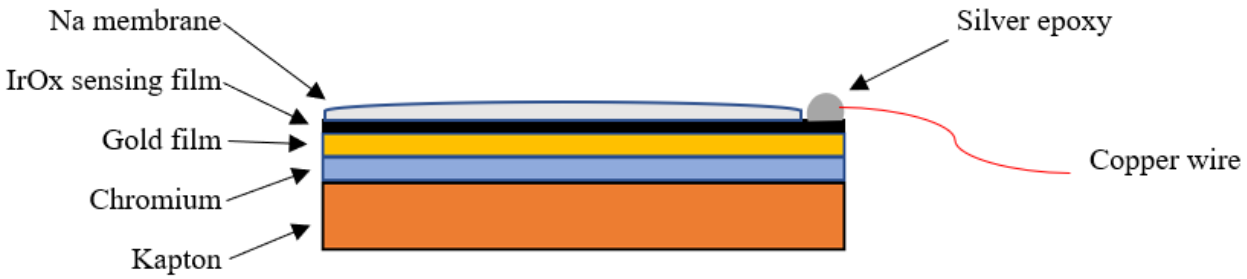

Fig 23 – Cross sectional view of an Iridium Oxide based Sodium sensor

2.4 Working of Commercial reference electrode

Commercial glass reference electrode has been used for all measurements in this chapter. Silver Chloride (Agcl) electrodes are used widely in developing biosensors due to their ability to transfer

current without loss. Commercial reference electrode comes sealed in a glass tube, the electrode silver is covered with silver chloride either physically, chemically or by electrochemical process. Silver- silver chloride electrode follows Nernst equation and the redox reaction involved is:

$$Agcl\ (S) \longleftrightarrow Ag^{+} + Cl^{-}$$

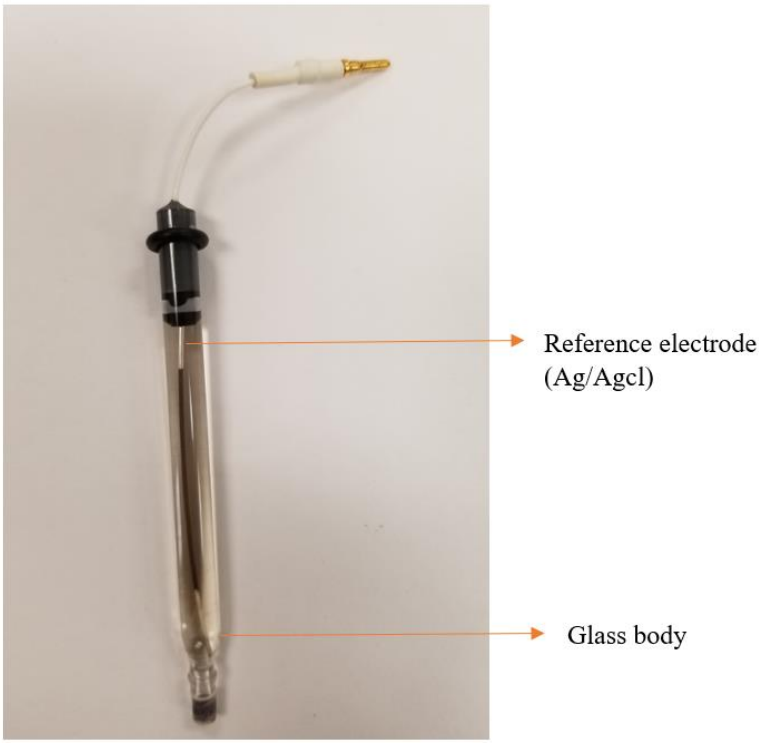

Fig 24 – Silver Chloride commercial reference electrode (MF-2052).

2.5 Discussion

From data comparison, type III exhibits highest sensitivity of about 60.3 mV/pH, type I and type II with sensitivity of 58.6mV/pH and 59.9 mV/pH respectively. Hysteresis study based on electrode size and initiation point of three electrode types were intensely investigated. Regardless of electrode type small smallest size had the least hysteresis. Hysteresis in type I electrode was

calculated to be highest, especially under condition when electrode is not washed in DI water. Investigation on response time of the sensors were found to be around six seconds, based on size and electrode type. Repeatability of sensor is an instrumental parameter in understanding if same performance can be repeated. All three electrodes of same size were tested for 20 and 40 cycles. Type I electrode is found to be most consistent but the other two types also shows consistent potential after 10 cycles. Influence of sodium ion on potential during pH reading was also studied. Although potential increases with salt concentration, sensitivity remains same.

Chapter 3

IRIDIUM OXIDE BASED PH SENSOR BY ELECTROPLATING METHOD

3.1 Fabrication process

3.1.1 Solution preparation

Iridium oxide film grown electrochemically exhibit high sensitivity with low response time accounting to the porous nature of the film. Electrodes of this types are widely known to show super Nernstian behavior. The film is deposited onto a flexible polyamide (127 μm) substrate, similar sample types discussed in Chapter 1. Recipe to make Yamanaka solution follows:

a. Anhydrous Iridium Chloride ($IrCl_4$) weighing 0.075g (Sigma-Aldrich) is mixed with 50 ml of DI water using a magnetic stirrer.
b. Further, 0.5 ml of 30% hydrogen peroxide (Fisher Scientific) is mixed into solution and stirred for 10 more minutes.
c. Again, 250 mg of oxalic acid (Caledon Laboratories) is mixed and left to stir for 10 more minutes.
d. Lastly, potassium carbonate (Sigma Aldrich) is added to pH level to 10. Commercial glass electrode is used to adjust the pH level of the solution and the solution is rested for 4 days.

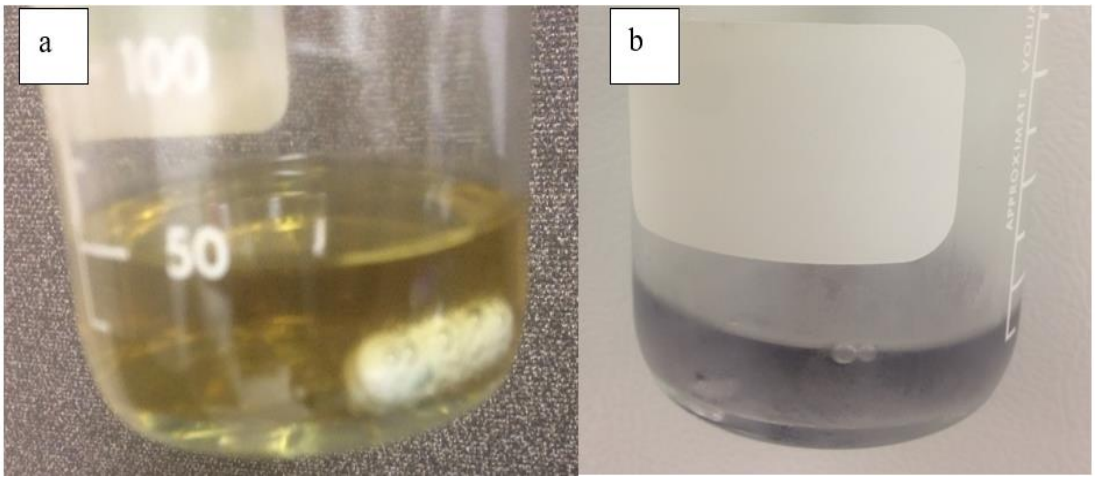

Figure 25- Solution color before (a) and after (b) four days

3.1.2 Sample preparation and instruments used

Samples discussed in Chapter 1 are cut into small stripes of area 1mm x 10mm. Copper wires of length 5 cm are attached to the samples using Silver epoxy which is a conductive and adhesive paste. It takes about 12 hours for silver epoxy to dry off properly. Next, samples are cleaned in Acetone to wash off any dust particles, Methanol to strip out foreign adhesive layers from the Au film and DI water for the final rinse.

Film is grown electrochemically on the working electrode using a Potentiostat (Model 700E, CH Instruments), a commercial Ag/Agcl reference glass electrode (MW-2021, Bioanalytical Systems Inc.) and inert metal Platinum is used as the counter electrode to complete the circuit. Varying potential between the WE and RE produces current for ionic movement and counter electrode platinum is used to complete the circuit.

3.2 CV plots and sensor performance

3.2.1 Chromium based samples

Type I samples discussed in chapter 1 is used, where Cr is the only adhesive layer between Au and Kapton substrate. 4 best electrodes are selected from a batch of 10 electrodes.

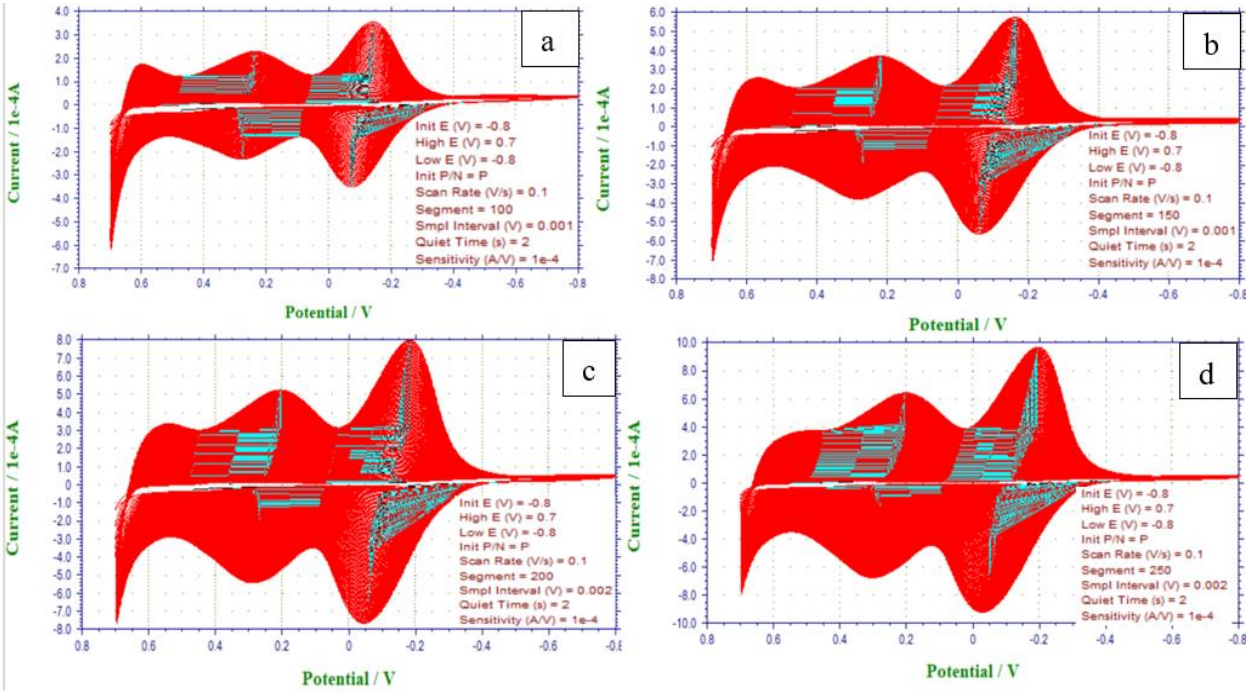

Fig 26 – Type I CV plots (a) 100 cycles (b) 150 cycles (c) 200 cycles (d) 250 cycles

Cyclic Voltammetry of 100, 150, 200 and 250 sweeps are performed to identify how optimum number of cycles can affect the sensor response.

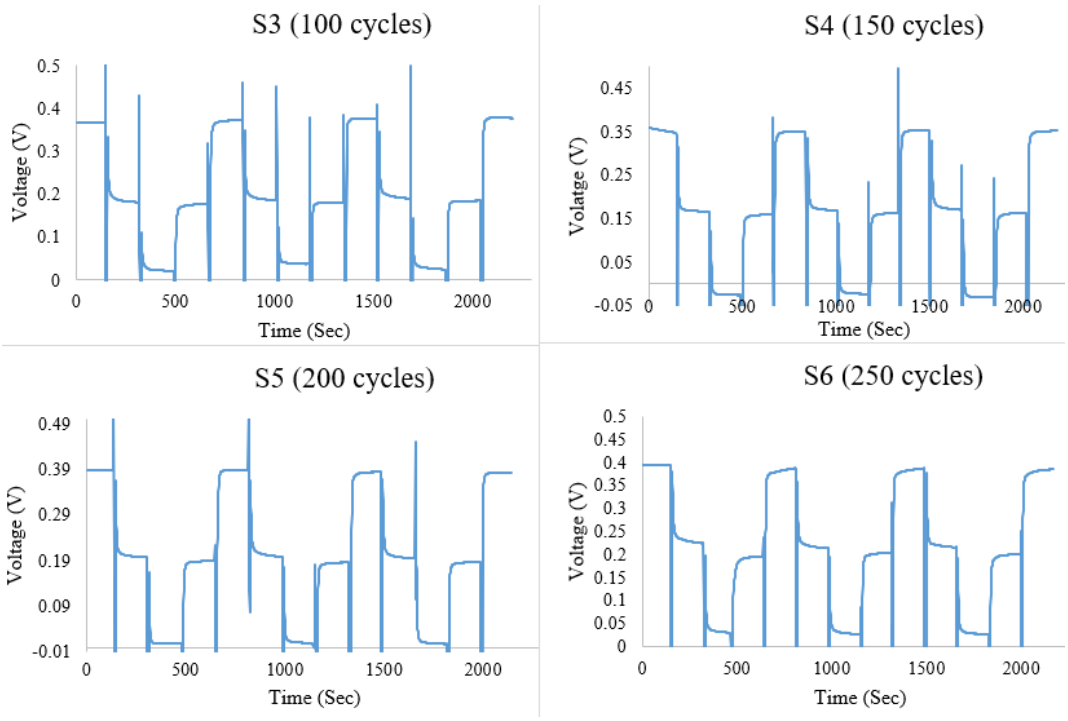

Fig 27 – Type I hysteresis plot at 100, 150, 200 and 250 cycles.

For hysteresis study, samples were tested at 3 pH levels pH 4,7, 10 and vice versa. Test was repeated 3 times by dipping electrodes at pH buffer solutions at 4-7-10-7-4.

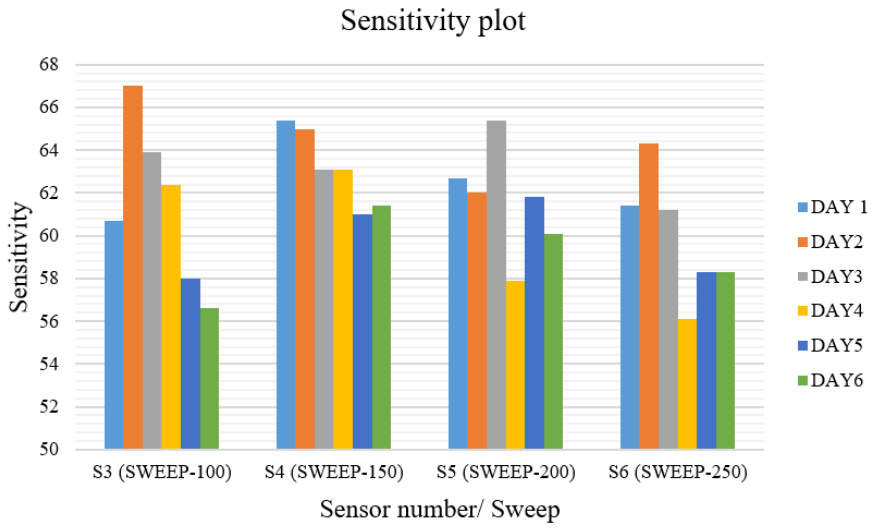

Fig 28 – Type I sensitivity plot tested for 6 days deposited with different number of sweeps/cycles.

From figure 28, it can be well said that the sensor is stable; repeatability test carried out for 6 days shows drifts in the potential. When Iridium Oxide is electrodeposited on Chromium based samples, Super Nernstian response can be achieved. This is credited to the porous nature of the film, allowing faster ionic exchange. Among all the other samples, sample number 4 subjected to 150 cycles shows a stable response.

3.2.2 Copper based samples

Type II and type III samples used in chapter 1 were fabricated from the NanoFab, UTA. Another new type of copper sample manufactured by Dupont has also been used to study sensor response.

3.2.2.1 Samples prepared in NanoFab, UTA.

Type II and type III samples have copper as one of the metal layers.

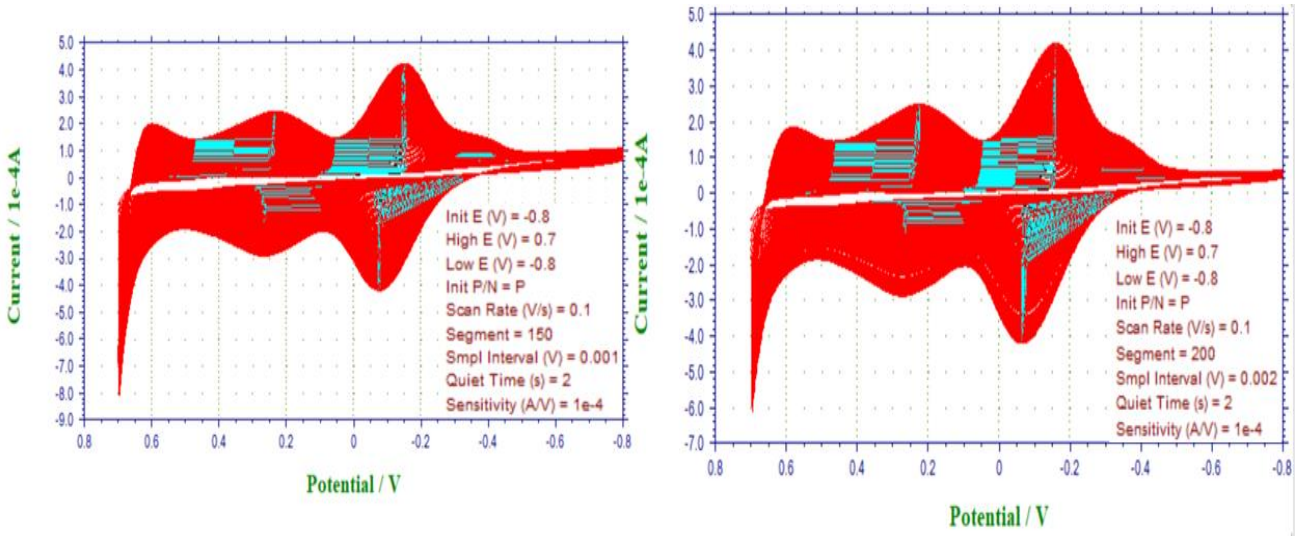

Fig 29 – CV plot for copper-based samples (type II and III) under 150 and 200 cycles.

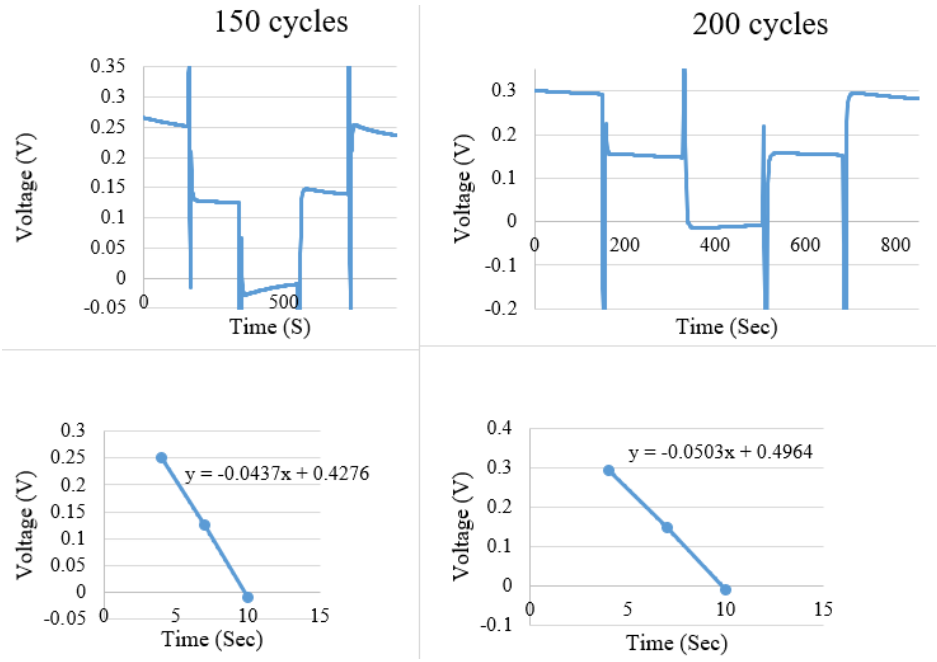

Fig 30 – Hysteresis and Sensitivity plot of samples (II and III) with 150 and 200 cycles.

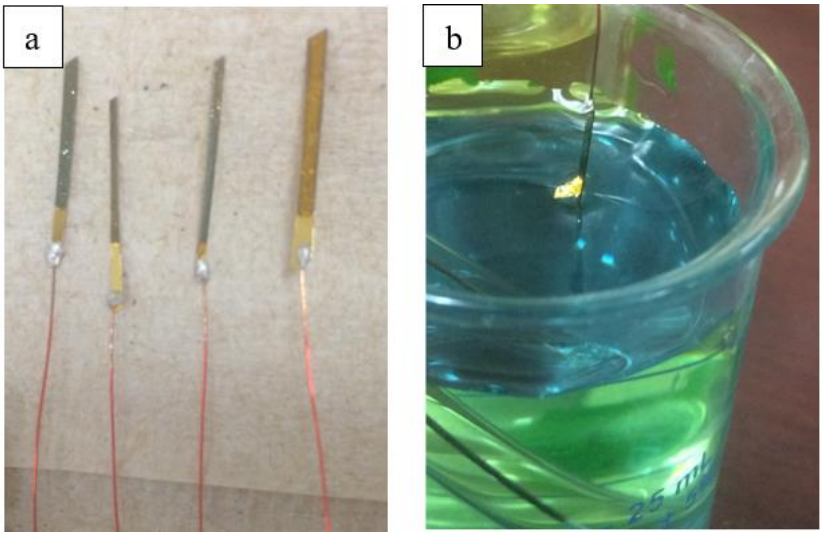

Fig 31 – (a) Cracked copper-based samples (b) Au layer peeling off during sensitivity tests

Sensitivity shown in fig [] is lower than expected. After the sensitivity tests, severe cracks on Au film and peeling off entire film were also observed. Because electrodeposition technique requires samples to be dipped in the solution for extended period, a plausible explanation for such outcome

could be because copper is not as adhesive as chromium. Therefore, failing to hold Au metal layer to the flexible polyamide substrate.

3.2.2.2 Dupont sample

Copper thickness of this sample is 17 µm, write specifications. The CV plot has been done within voltage range of -0.8 V to 0.7 V for 50, 80 and 100 cycles. Hysteresis and sensitivity study were also done accordingly.

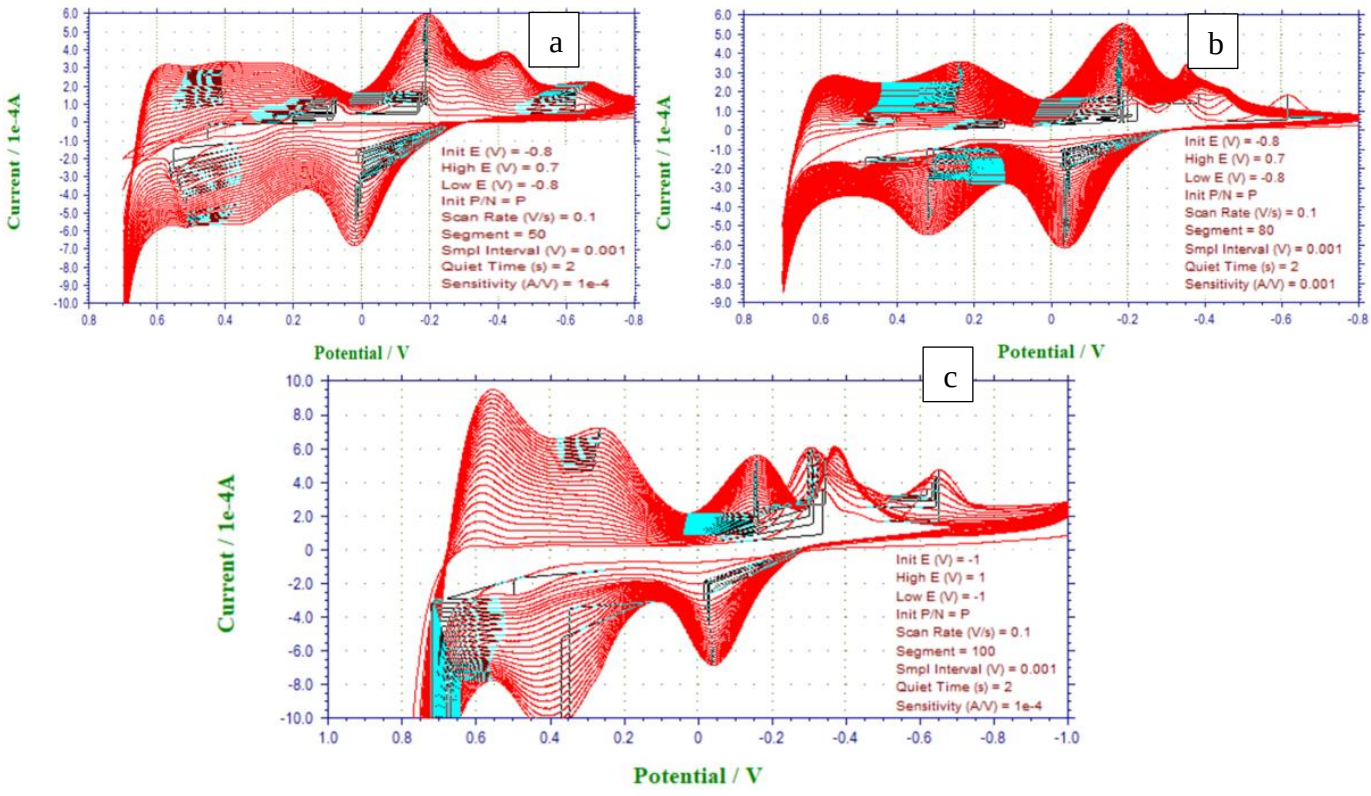

Fig 32 – Dupont samples CV plot for (a) 50 cycles, (b)80 cycles (c)100 cycles

Sensitivity and hysteresis study were performed by dipping the sensors in different buffer levels of pH 1,4,7,10,13 and vice versa. The sensor failed to respond in high acidic solution. Study on these samples were not a success probably due to the thickness of copper layer and thin layer of Iridium oxide sensing film. From CV plots also it can be predicted that beyond 80 cycles, sensor

response becomes enigmatic. Recognizing optimum voltage range is also integral for a sensor to perform well. Anomalous voltage range can be disrupting for the samples. Plot below is an example of how hysteresis response looks like in this study and a high increase in voltage range.

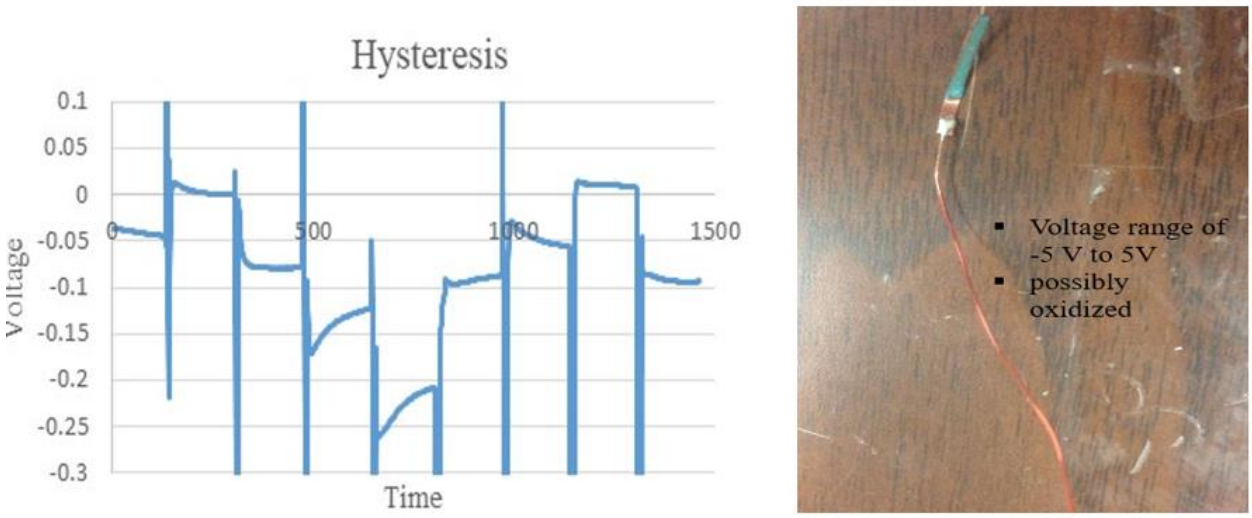

Fig 33 – Dupont sample (a) Hysteresis plot (b) High voltage range

3.3 Discussion

Comparing CV plots and sensitivity tests, it can be noted that study on Cr based sample (Type II) was a success but Cu based samples failed. Type II samples also exhibited super Nernstian response, and stable response at 150 cycles. Unfortunately, the results could not be repeated, and the sensor performance started deteriorating as shown in fig []. Cu based electrodes suffered from severe cracks and film peeling away. For these reasons, study on Iridium based Oxide electrode by Electrodeposition could not be carried out further. But high sensitivity of such electrodes is still of interest and further investigation could be done in the future.

Chapter 4

DEVICE PACKAGING

4.1 Packaging process

Materials used during packaging process is listed, information such as thickness and operating temperatures are also itemized. Raw materials were purchased from amazon. Design specification has been collected from user manual or company website.

Material	Thickness (mm)	Operational/melting temperature (ºC)
Lamination pouch	0.0762	110
Double tape	~0.0762	121
Electrode	~ 0.127	400 (kapton)

Table 3 – Material information

Very often device packaging is a serious problem in production phase. Many existing devices cannot be marketed due to packaging problems and cost inefficiency. This chapter of research focuses on device packaging and sensor performance thereafter. A design flow is included which requires only cheap materials and will allow large scale production with cost effectiveness.

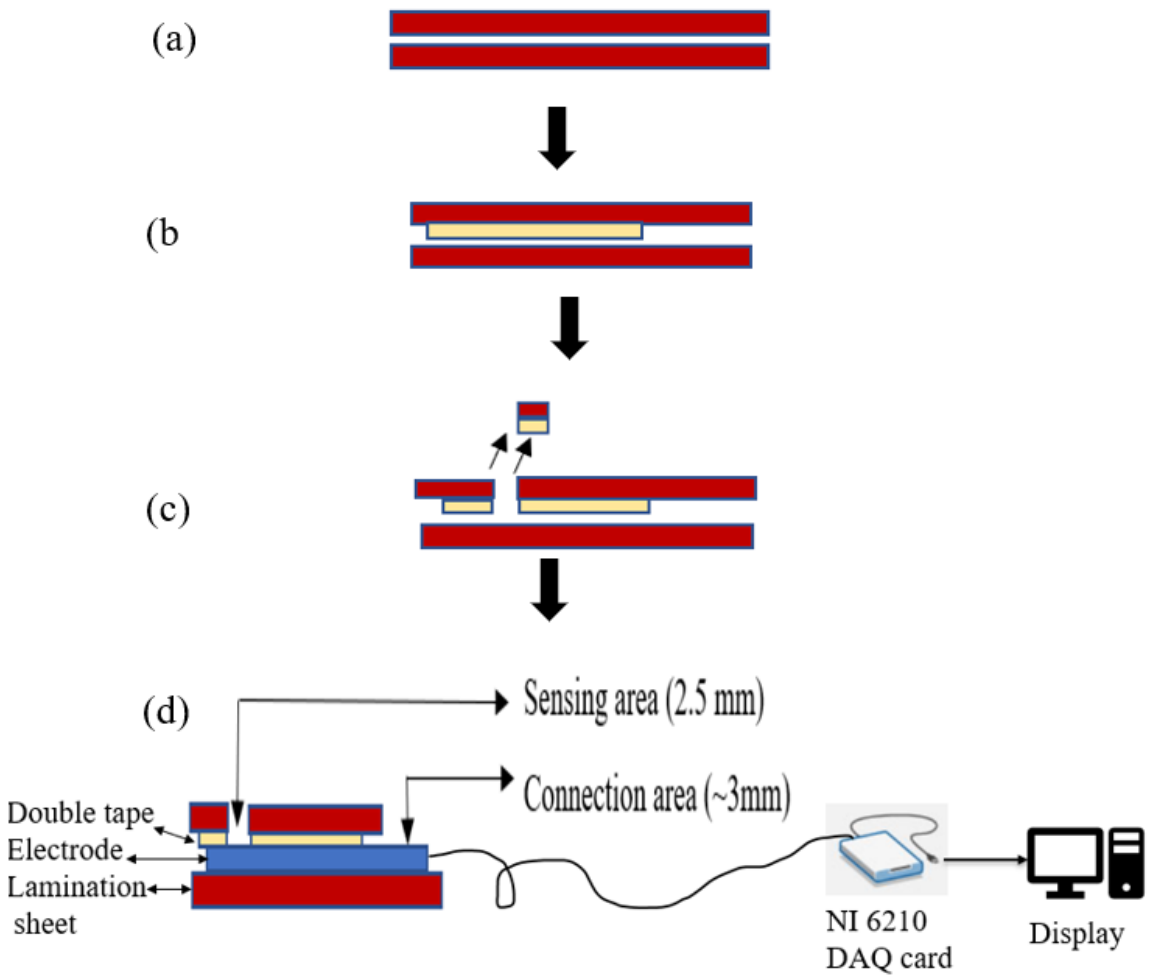

Fig 34 – Design flow of device packaging. (a) laminating pouch, (b) double tape, (c) window punctured out using biopsy punch, (d) Data acquisition from a laminated sample.

4.2 Approaches to develop sensing window

4.2.1 Laser Cutter

To efficiently cut out sensing window in mass production, a laser cutter available in Central Library, UTA was used. Maximum laser power is 50 W and optimum power level is 50%, so to acquire finer edges, an optimum power level of 25 W was used.

No	Sensing window dimension (mm * mm)	Distance between electrodes (mm)	Status
1	0.5 * 0.5	2	No response
2	1 * 1	2	No response
3	1.5 * 1.5	2	No response
4	X * Y	<2	During lamination difficult to create isolation between the RE and WE

Table 4 – Trials in developing sensing window using laser cutter.

Fig 35 – Real time current reading by NI DAQ card.

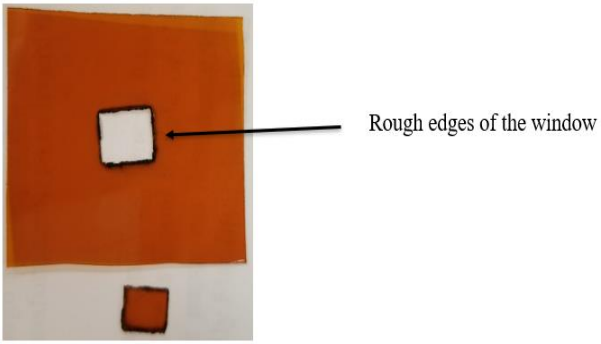

Fig 36 - Sample with rough edges using laser cutter.

From table [], Fig [] and [], it can be noted that this trial was not successful. Failure could be potentially because of sensing window being extremely small and rough edges in the polyamide film. These factors could have resisted interaction between the buffer solution and Iridium Oxide. It is also clear from current real time reading in Fig [] that random reading is being picked. To also maintain physical isolation between the reference (RE) and working electrode (WE), the optimum distance studied is 2 mm.

4.2.2 Surgical blade

Using a surgical blade solved problem of rough edges. An optimum distance of 2 mm between the WE and RE was maintained, and crocodile clippers were used for conductivity.

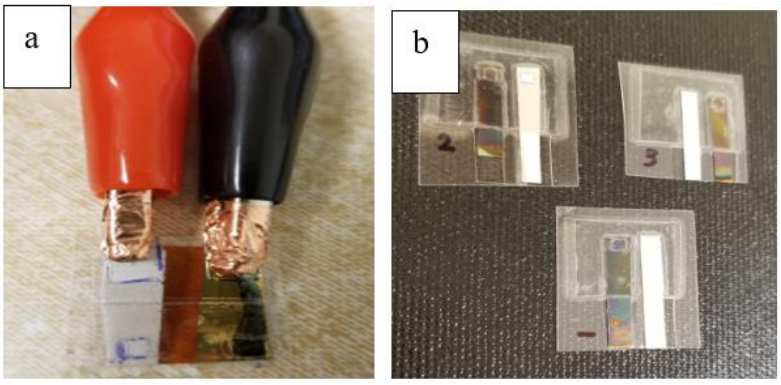

Fig 37 – (a) Crocodile clippers wrapped in copper foil (b) Laminated sample using surgical blade.

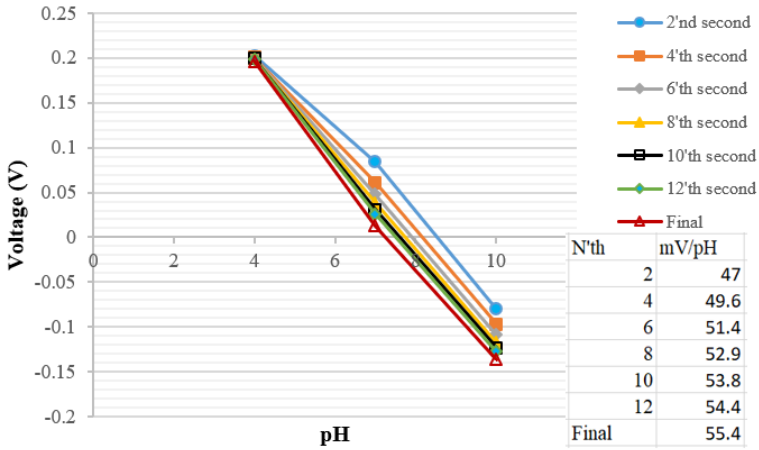

N'th	mV/pH
2	47
4	49.6
6	51.4
8	52.9
10	53.8
12	54.4
Final	55.4

Fig 38 – Sensitivity and response time plot.

From fig [], sensor packaging is a success, but response is slow. Sensitivity of the sensor slowly increases along with time soaked in the buffer solution. When samples are not packaged, it takes about 2 secs for sensor to give a stable reading, but laminated samples show a response time of 12 seconds.

4.2.3 Position of window

A hypothesis study of, position of the sensing window on the electrode being a factor for slow response of the sensor was performed. Two batches of sensors were prepared: (a) where sensing window is on the middle of the electrode, (b) where it is cut in the edge corner.

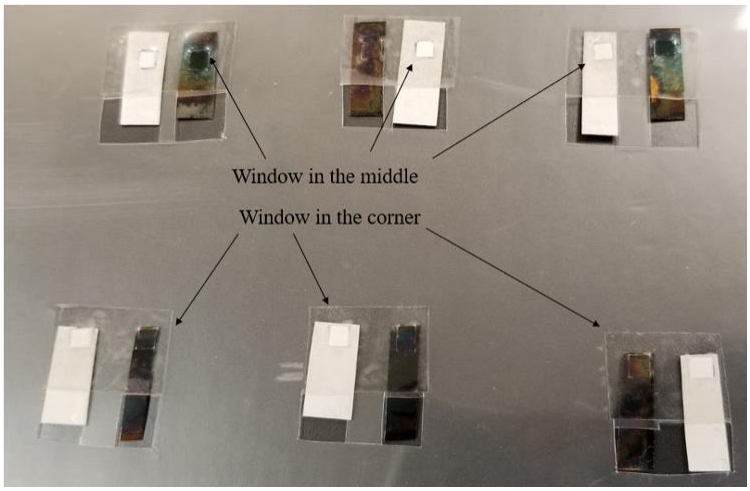

Fig 39 – Position of sensing window.

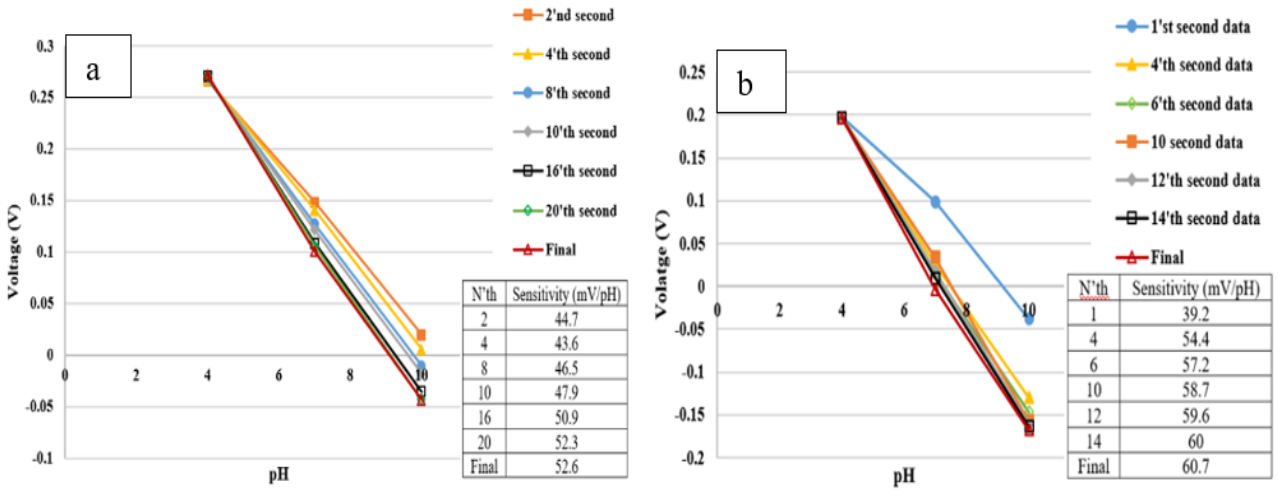

Fig 40 – Sensitivity and response time plot of (a)Window in the middle (b) Window in the corner.

In unlaminated samples and corner window model, tip of the electrode dipped, functions as the sensing area. Hypothesis on position of window on the electrode is found to be true; electrode with window in the corner has a faster response by 6 seconds as seen in fig 40. However, there may be other superior factors responsible for slow response of the laminated samples. So, further experiments on laminated samples with the corner window model is implemented.

4.2.4 Punch plier

Using a surgical blade to open window size of 2mm x 2 mm is quite tedious, so for the sake of convenience, using a punch plier has been opted. Sensor performance is like the ones when blade is used, response time is high.

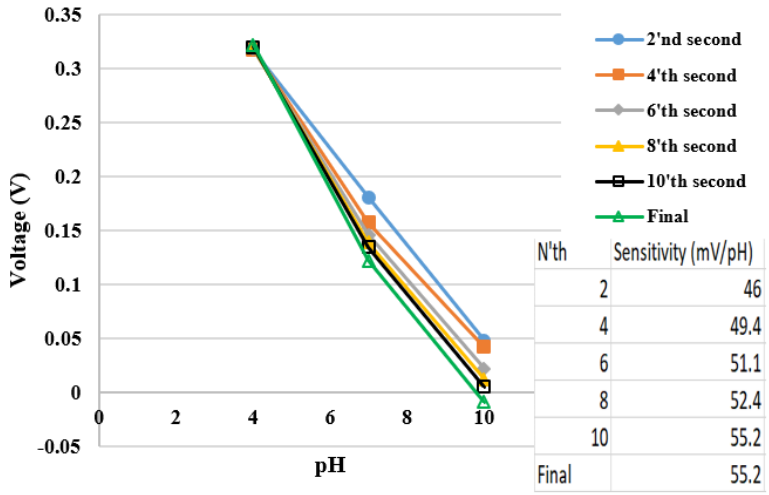

N'th	Sensitivity (mV/pH)
2	46
4	49.4
6	51.1
8	52.4
10	55.2
Final	55.2

Fig 41 – Sensitivity and response time of punch plier samples.

4.3 Response time study

For all laminated samples, even though sensor show response, it is slow and shows high hysteresis. To mitigate this problems, magnetic stirrer was used to increase the hydrodynamics of the solution. By doing so, the molecular interaction is higher and thereby we can expect precise reading.

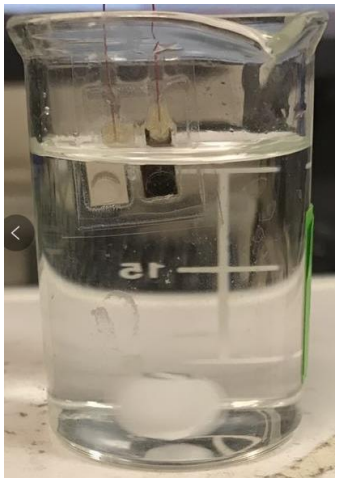

Fig 42 – Demonstration how laminated samples are tested in presence of magnetic stirrer.

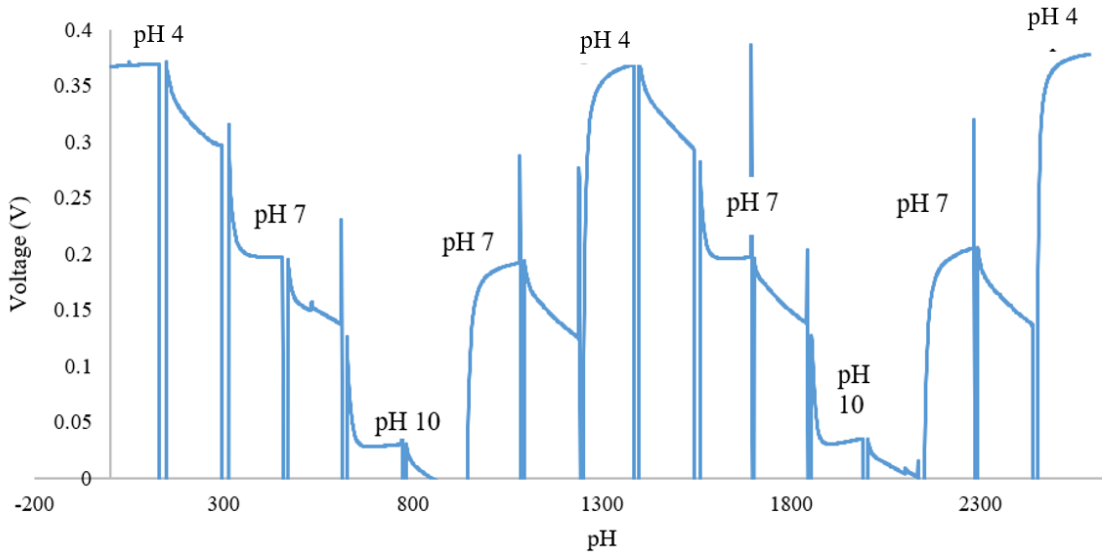

Fig 43 – Saturation time study, by running 2 cycle hysteresis tests, with DI wash.

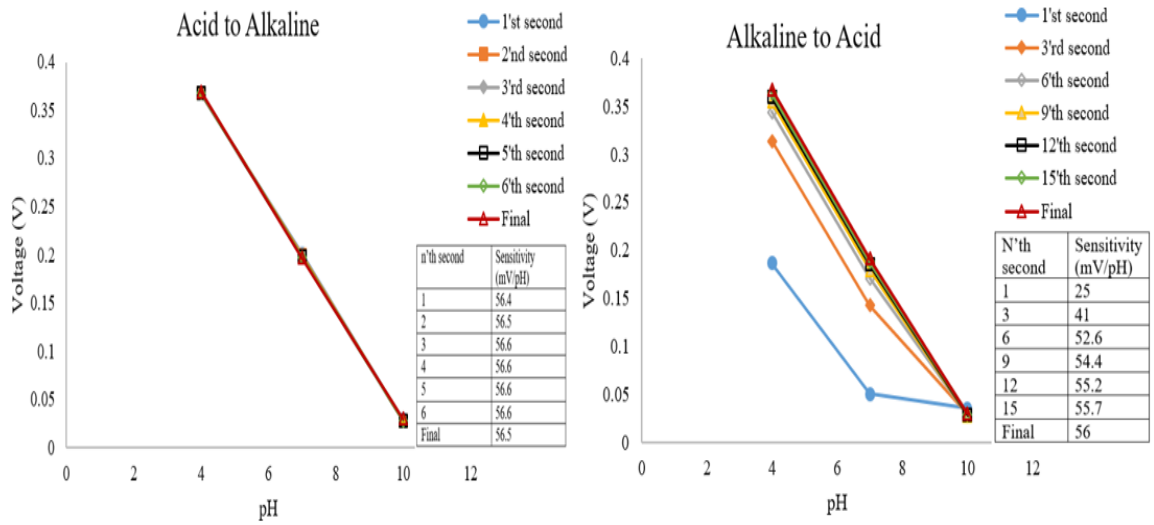

Fig 44 – Sensitivity and response time study.

A batch of 3 sensors were prepared to have a deeper understanding. Two cycle hysteresis study with DI wash was done, using a magnetic stirrer at pH buffer solution pH 4,7 and 10, and vice versa. From fig 43 and 44, the hysteresis and response time of the sensor improved. Acid to alkaline has a faster response over alkaline to acid response.

4.4 Skin test

Skin test has been performed by using a wet cotton and dapping it onto the sensor. Sample is laminated, windows for RE and WE are opened using a biopsy punch, with a diameter of 2.5 mm. Healthy skin has a pH value of about 5.5; deviation from this value can allow fungal growth contributing to skin sensitivity such eczema or rosacea. Skin pH is corelated to tissue health and the need for deeper understanding their correlation, is becoming a topic of interest in the medical and cosmetic industries.

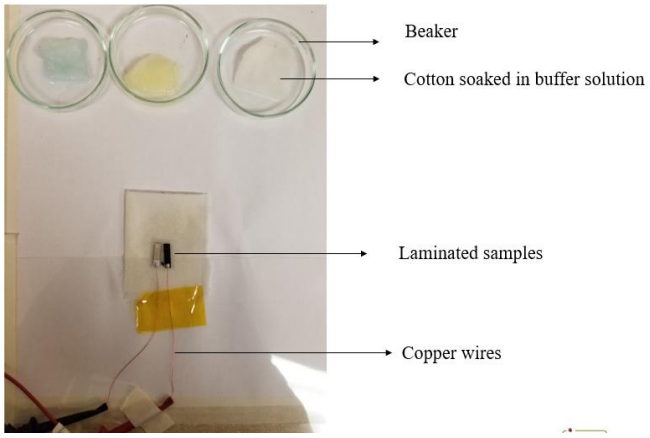

Fig 45 – Skin test set up.

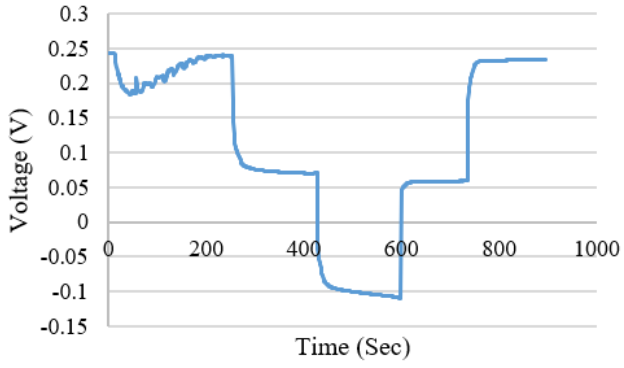

Fig 46 – Hysteresis study for skin test at buffer pH 4,7, and 10.

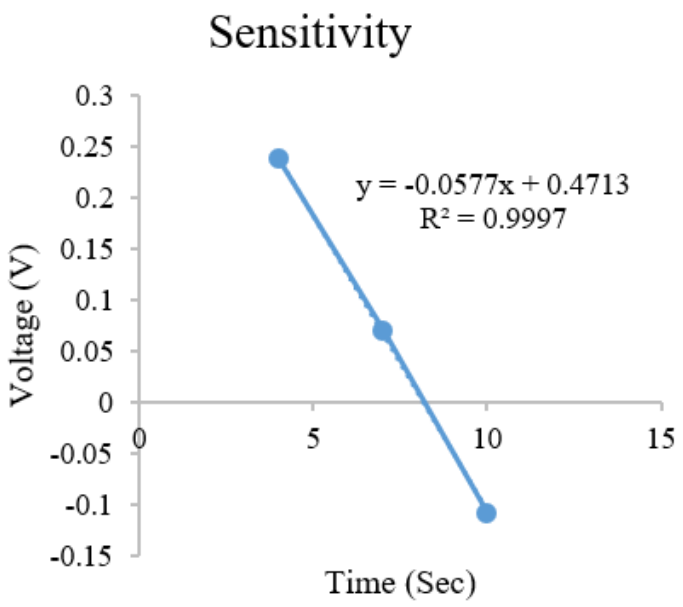

Fig 47 – Sensitivity plot tested at buffer pH 4,7,and 10.

4.5 Discussion

Developing a laminated sample has been a challenge, especially device performance after the laminating process. Regardless of sample type, all laminated samples suffered from severe hysteresis and response time. Using a magnetic stirrer has helped mitigate hysteresis problem and response time hence, improving device performance. However, because hydrodynamics of the solution speeds up, it also generates noise. To avoid noisy data, we can use an array of electrodes with an extra RE to cancel out the noise. Samples where punch plier is used to open sensing window has shown best performance. With recommendations from experienced researchers, punch plier was replaced by biopsy punch for convenience; both tools can create fine edges and exhibits similar response.

Chapter 5

LAMINATED SENSOR ARRAY

5.1 Objective

Biofluids reserve a plethora of biomarkers, inability of the human body to excrete biofluids continuously or in high quantity remains a challenge. Retrieving information present in Interstitial fluids such as sweat, tears and saliva can boost minimally invasive or non-invasive technology. So far, real time monitoring of sweat to study diabetic condition in a patient has been most successful. Using tear as the analyte, research demonstrates how continuous health monitoring can be inefficient due to inability of human body to secrete enough fluid. While Saliva is a good option which is quickly accessible, the real challenge is that, pH level of the fluid differs among different areas of the mouth. Therefore, this chapter of research has focused on sweat as the analyte of interest to perform biochemical sensing.

Emerging peripheral devices depends on external biofluid and allow patients to carry labs with them for real time health monitoring. Implantable devices serve the same purpose but are used for biochemical sensing of the internal organs. The later technology remains uncertain due to challenges such as patient discomfort, possibility of infection, and electromagnetic interferences.

It has been demonstrated in chapter 2 that presence of ions can influence potential generated thereby effecting the pH reading. Therefore, it is crucial to distinguish potential generated by sodium and hydrogen ions. Integrating two working electrode (WE): pH and sodium, and two reference electrodes (RE) can help distinguish the potential generated by respective Wes. Noise generated can be cancelled out by subtracting potentials between the two respective Res.

5.2 Sensor fabrication

Fabrication of pH and sodium sensing working electrodes are based on IrOx film. For sodium electrode, an additional layer of sodium ion selective membrane is coated on IrOx film. As discussed in chapter 2, these electrodes are developed using Sol-Gel or the dipping method.

Commercial reference electrode is bulky and inconvenient for device integration, so a traditional way of developing miniaturized reference electrode using Ag/Agcl paste is employed. A polyamide Kapton film of thickness 127 µm is washed in acetone and methanol to strip off dust particles or existing adhesive layer on the sample. Next, sample is dried either by nitrogen blow, air drying by leaving it on hot plate or patting it with a clean tissue paper which does not generate particles. Although, leaving samples to air dry on hot plate causes rings on the samples, at temperature slightly higher than room temperature. So, this option is often discarded. Further, the Ag/Agcl paste is manually applied on the clean samples with the help of other clean samples strip. Finally, coated sample is left on the hot plate for ten minutes at 125 ºC for the paste to dry and after samples are cooled, they are cut into strips of desired dimensions. A regular sharp pair of scissors can be used to complete this step.

Sensors of size 2 mm x 5 mm are integrated into a single sample and laminated, similar procedure as discussed in chapter 4. pH working and silver chloride reference electrodes are placed opposite to each other and sodium sensor is placed in between the two reference electrodes. To minimize noise generation between the two Res, they are placed farthest from each other. Biopsy punch of diameter 2.5 mm is used to open sensing windows, copper wire and silver epoxy are used for conductivity, and distance of 2 mm is maintained between adjacent electrodes. In the model sample, an electrode for Lactate sensing is also developed. Developing an array of sensor was done

in collaboration with a colleague and this part of research has focused on pH channel (WE_1) and sodium channel (WE_2). Therefore, there is no report about the third channel (WE3) in this thesis.

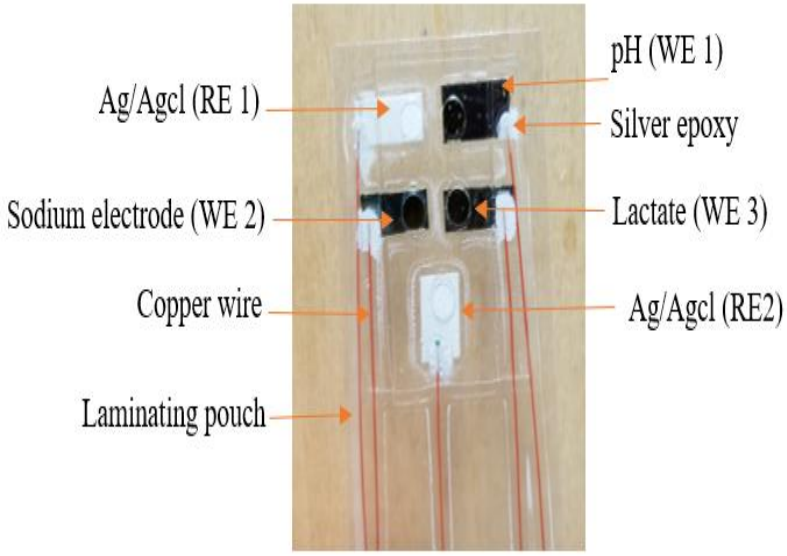

Fig 48 – Sensor array.

5.3 Results

A trial test was conducted to realize if electrodes integrated together can work simultaneously. Arrangement of electrodes is as shown in fig48; three working electrodes placed adjacent to two other reference electrodes. NI DAQ card 62100 series is used for data acquisition and LabVIEW programming is used to acquire data at the rate of 7data points per second.

Because all the three working electrodes share a common ground and same medium, they share the same environment. Before stepping into the real project, it was important to understand if there is uniformity between the working electrodes. So, three Iridium Oxide based electrodes were arrayed with two other reference electrodes and tested at buffer solution pH 4, 7 and 10.

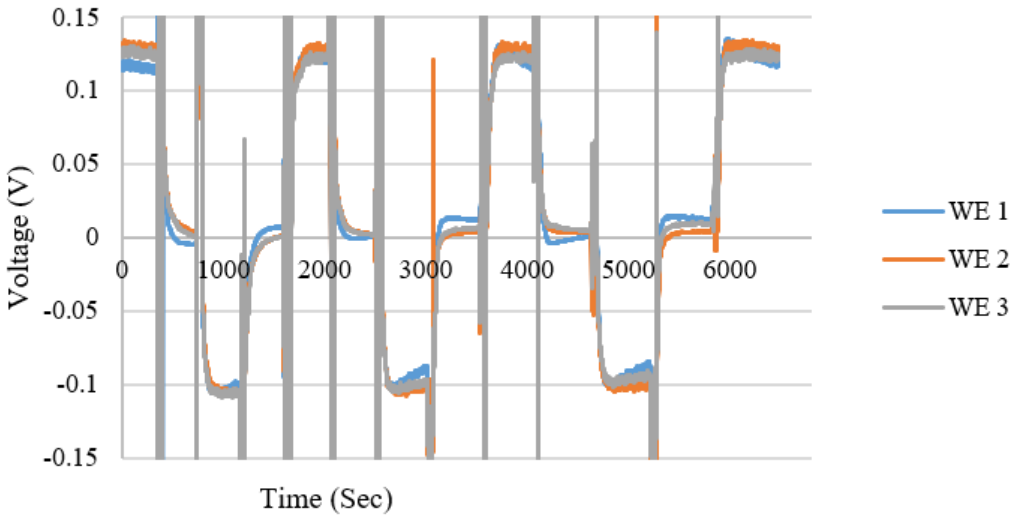

Fig 49 – Uniformity test between working electrodes.

Sample was tested in buffer solution (with pH 4-7-10-7-4) for three continuous cycles. All three electrodes were connected to common ground (RE_1), and 3 channel data were recorded simultaneously. The existing potential variation among the working electrodes can be improved by introducing a fourth channel which is the noise channel. Potential difference between the two reference electrodes (RE_1 and RE_2) is used as the noise channel.

5.3.1 Sodium sensor

Sodium ion concentration in the human sweat ranges from 10mM to 90mM. Composition of artificial sweat exhibits huge quantity of sodium ions. Therefore, adding sodium chloride salt to artificial sweat with sodium concentration of 10mM to 90mM was ineffective, due to the high amount of existing sodium ions. To understanding working of sodium sensor, testing solution of DI water with different salt concentration from 10mM to 90mM was prepared.

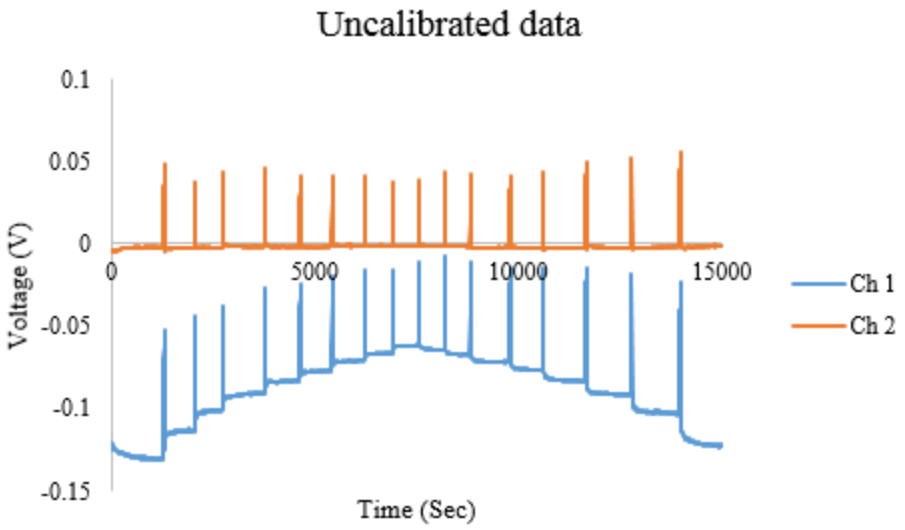

Fig 50 – Uncalibrated data

Ch 1: Potential between the sodium sensor WE and Ag/Agcl RE

Ch 2: Potential between the Ag/Acl RE_1 and Ag/Agcl RE_2

Data is calibrated by = $V_{Ch\,1} - V_{ch\,2}$. Calibrated data has reduced voltage overshoot, but hysteresis problem is not eliminated.

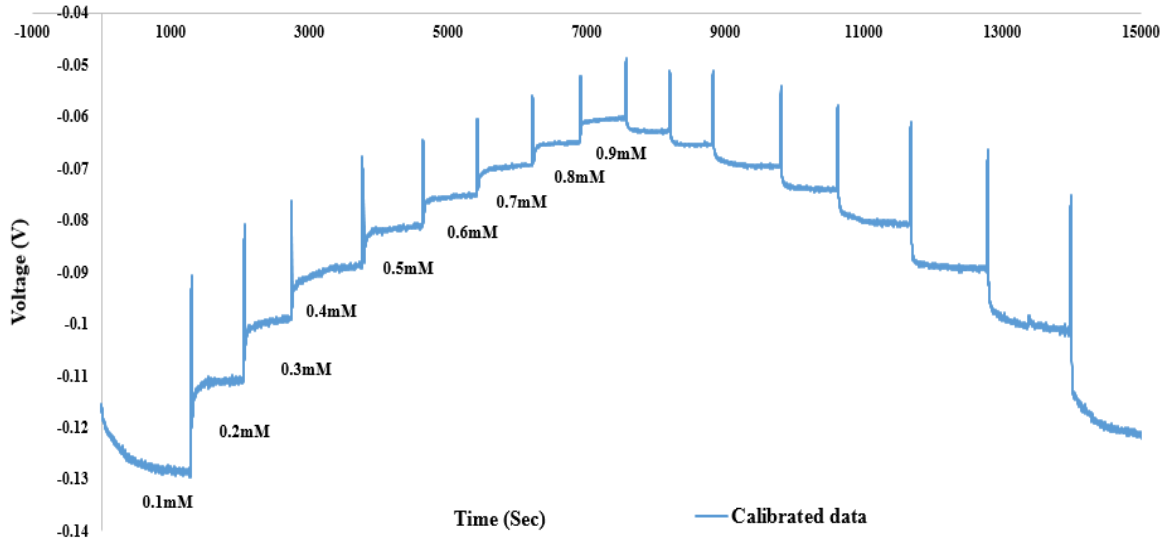

Fig 51 – Calibrated data.

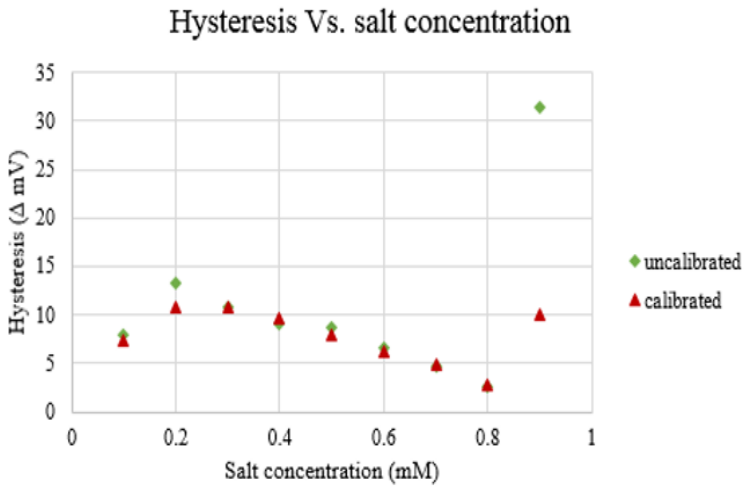

mM	uncalibrat	calibrated
0.1	7.958864	7.355498
0.2	13.22497	10.88706
0.3	10.7216	10.88008
0.4	9.03979	9.74314
0.5	8.782776	7.966966
0.6	6.612253	6.268922
0.7	4.60985	4.802931
0.8	2.658169	2.70797
0.9	31.33612	9.981297

Fig 52 – Hysteresis plot of sodium sensing channel.

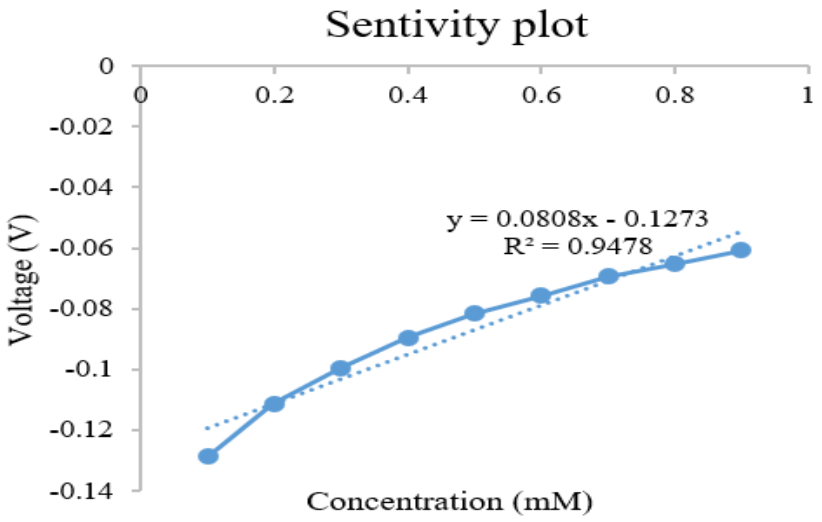

Fig 53-Sensitivity plot of sodium sensing electrode

5.3.2 pH sensor

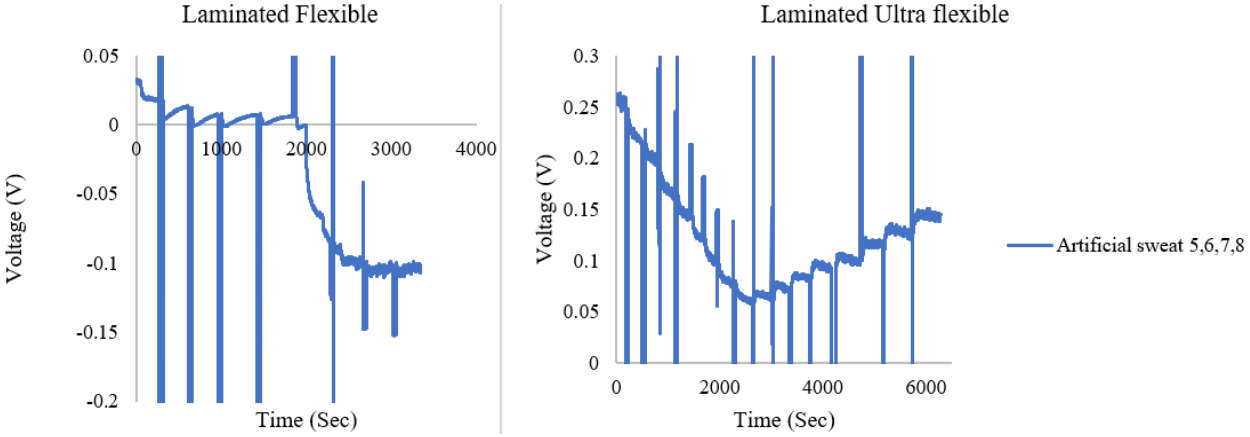

Fig 54 – A flexible and ultra-flexible electrode tested in artificial sweat.

Analyzing the graphs, it is not sure why laminated sensors did not respond. So, an intensive study was carried out.

5.3.2.1 Hydration problem

Electrodes that are not hydrated properly can suffer from hysteresis, voltage overshoot or slow response. To solve this problem, a laminated sample was tested in artificial sweat at pH 5,6,7,8 and vice versa for four continuous cycle. To increase the hydrodynamics, magnetic stirrer was used, rotating at 500 rpm. Samples did not respond because iridium Oxide film starting to peel away since a continuous test of four cycles took eight hours at a stretch.

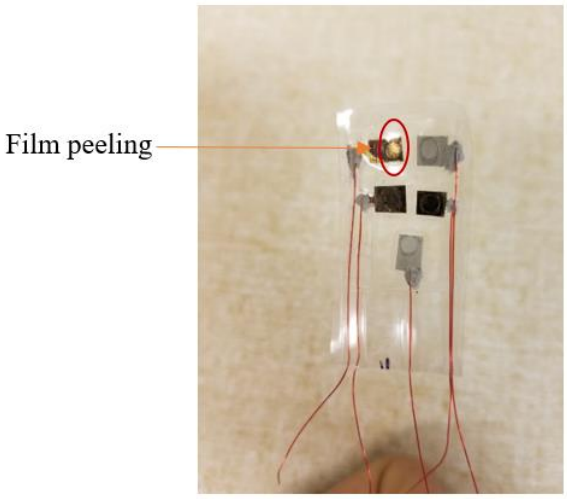

Fig 55 – Film peeling image when tested for 4 cycles (eight hours).

5.3.2.2 Size of sensing window

When insulation created is not proper, solution can leak through the sensing area and react at the connection point. To avoid situations demonstrated in fig [], samples with proper insulation is created and tested in buffer and artificial sweat.

Sample worked fine in pH buffer solution but suffered severe hysteresis in artificial sweat. An observation while working with samples; artificial sweat solution is more viscous than pH buffer solution. Viscosity of the solution could be the reason for severe hysteresis.

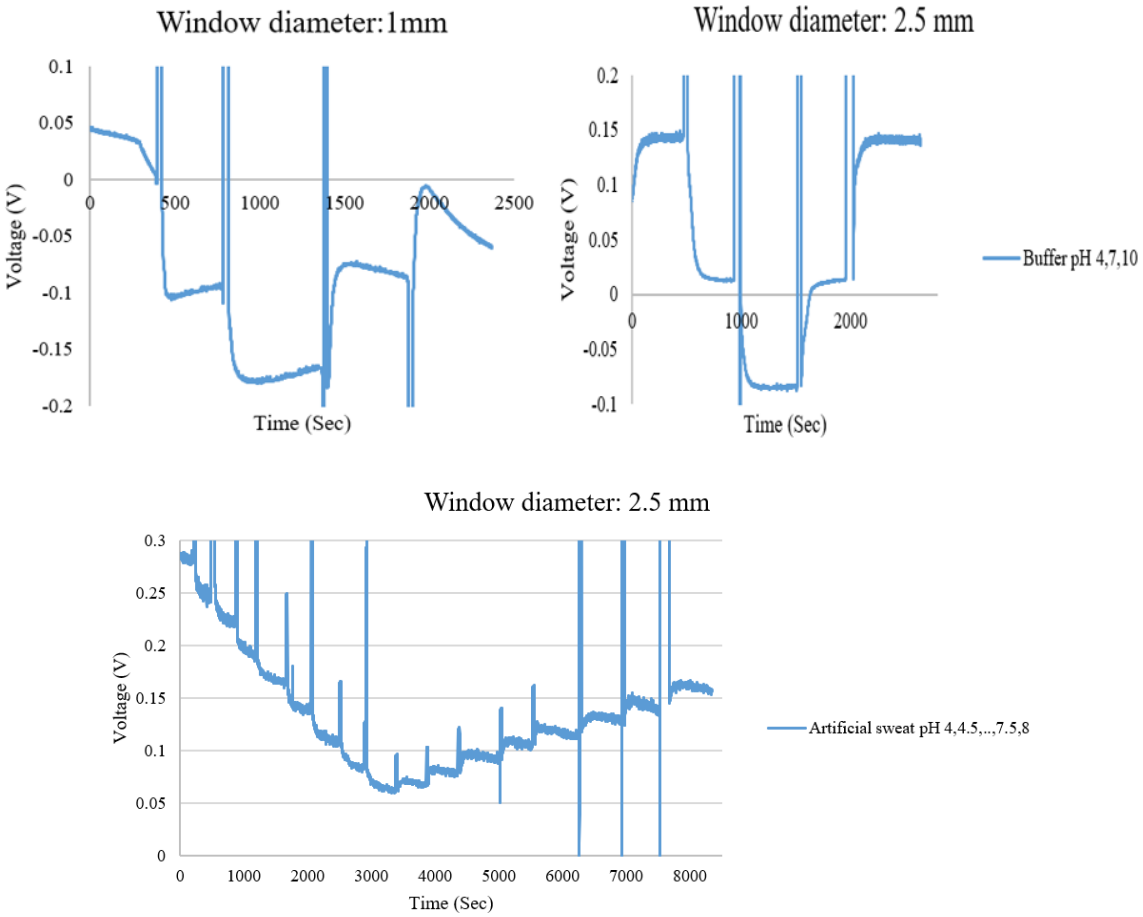

Fig 56 – Effect of window size on sensor performance.

5.3.2.3 Insulation problem or electrode design

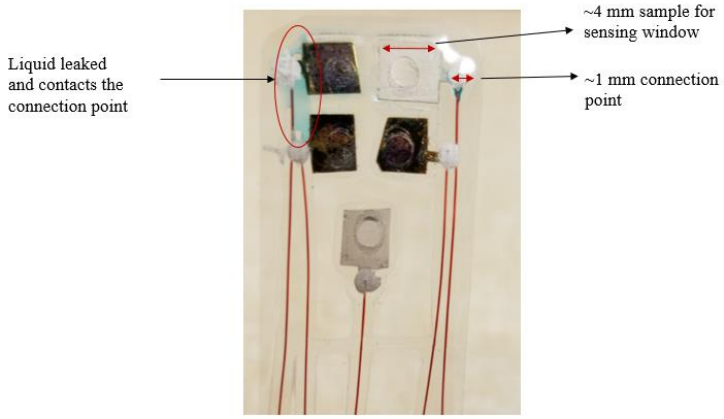

Fig 57 – Improper insulation.

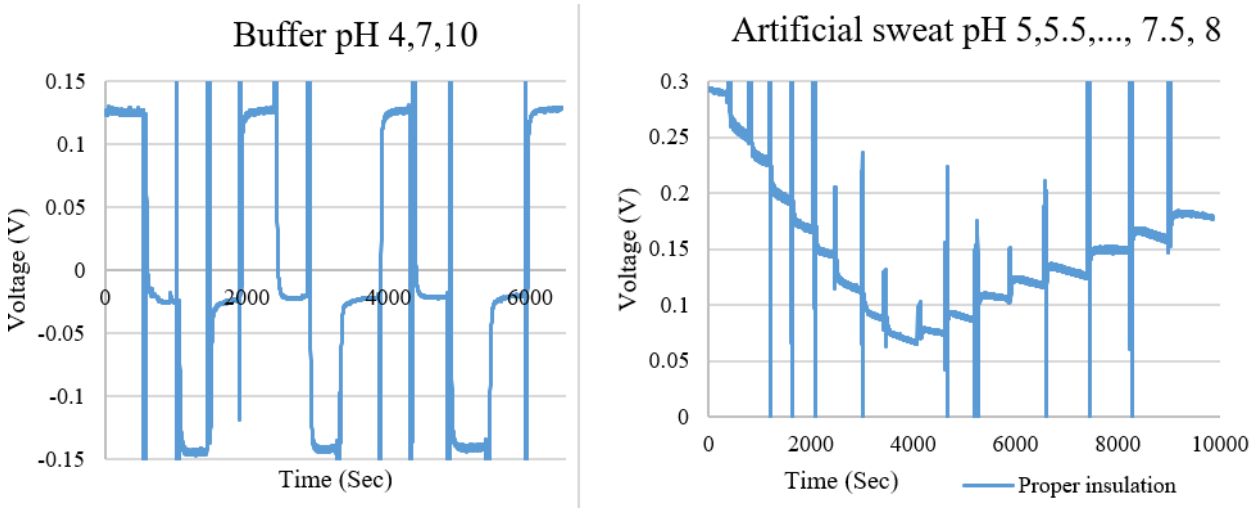

Fig 58 – Hysteresis study of sensor array with proper insulation.

5.3.2.4 Sample contamination (RIE treatment)

Steps involved in sample lamination deals with multiples hand handling activities and sliding through the laminator. Considering a hypothesis that sample contamination could have occurred during packaging process, a thorough investigation was done. To clean the laminated samples, they were introduced to low frequency plasma chamber. In the chamber, samples are cleaned in presence of oxygen, for 60 seconds.

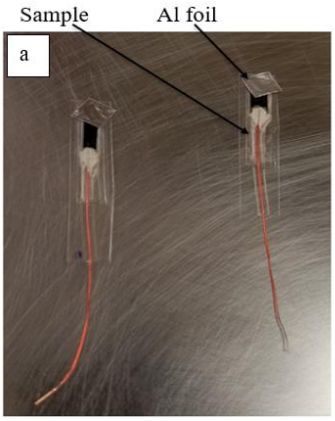

Equipment	RIE Macro 8800 (low frequency generator)
Gas	02
Etch power	750 Watts
Etch time	120 Sec
Pressure	150 mT

b

Fig 59 – (a)Sample in plasma chamber, (b) tool information.

5.3.2.4.1 Hysteresis and Sensitivity study part I

a. Testing solution

I. Buffer: pH 4,7,10

II. Artificial sweat: pH 5,6,7,8

III. Artificial sweat: pH 5,5.5,6,6.5,7,7.5,8

b. Conditions

I. Before lamination, before Plasma treatment

II. After lamination, before Plasma treatment

III. After lamination, after Plasma treatment

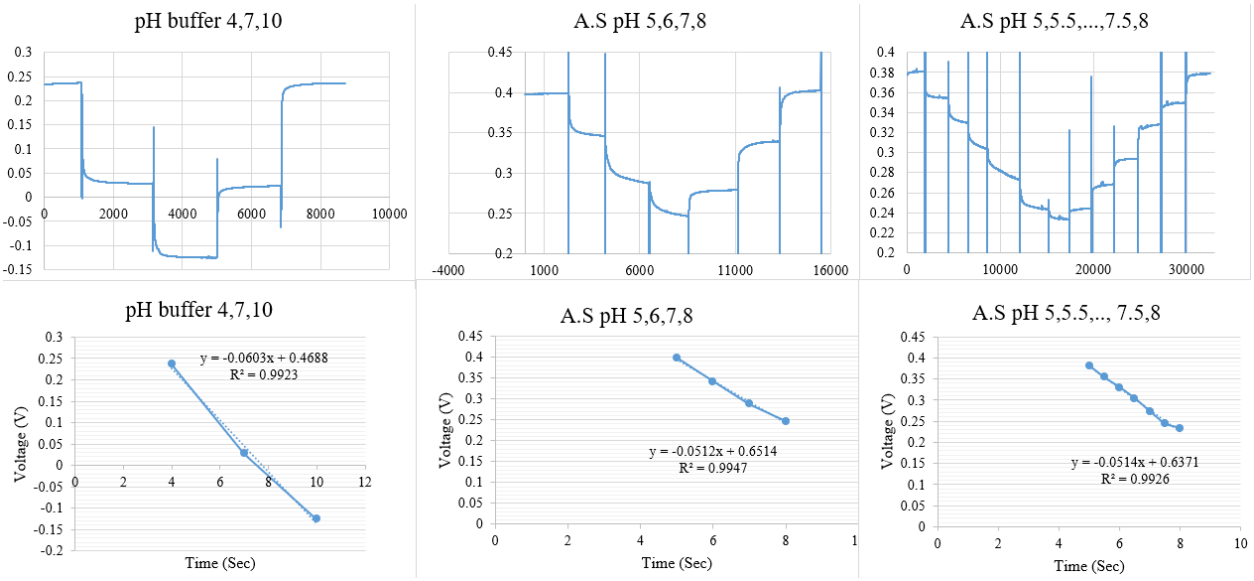

Fig 60 – Hysteresis and Sensitivity plot before lamination, before plasma treatment.

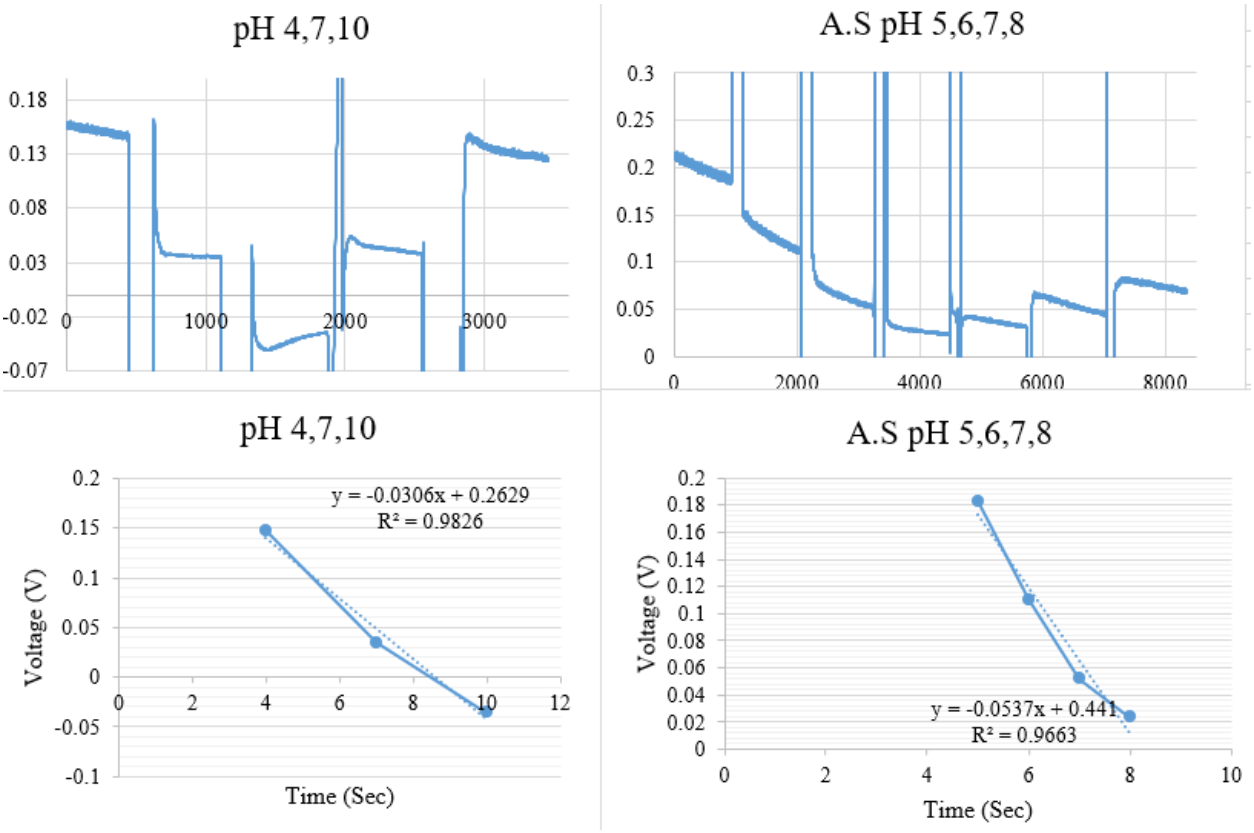

Fig 61 – Hysteresis and Sensitivity plot after lamination, before plasma treatment.

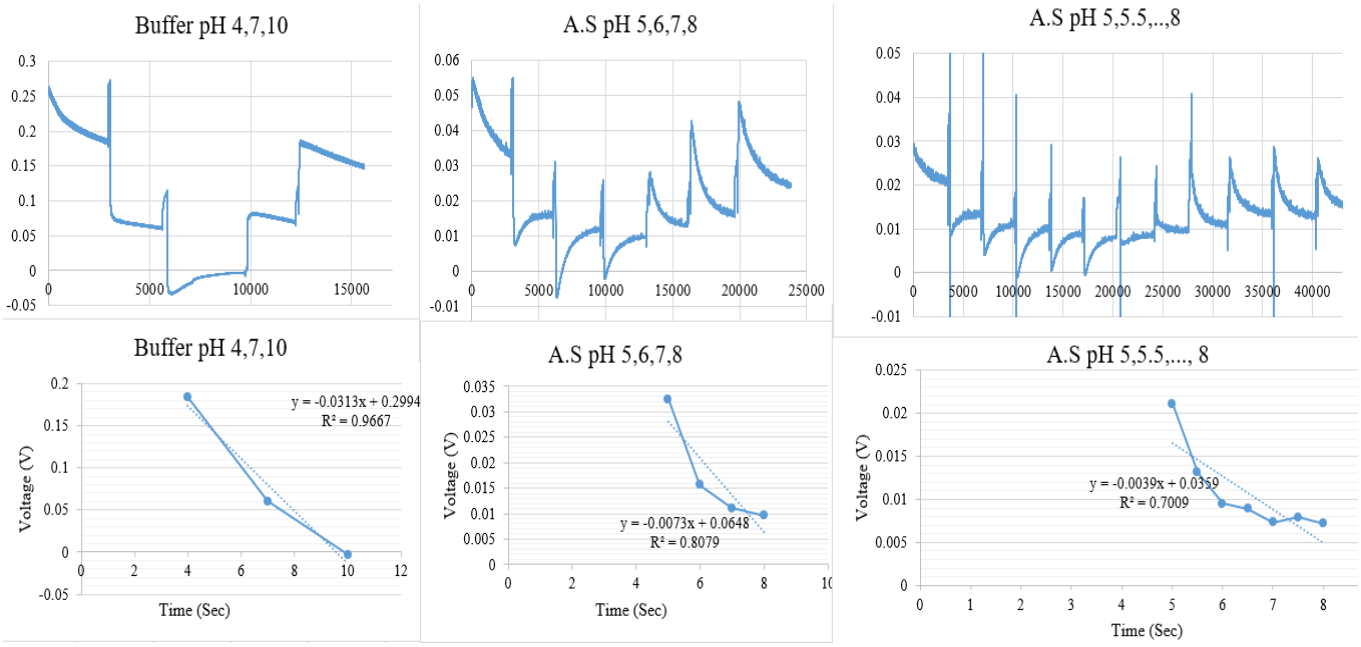

Fig 62 – Hysteresis and Sensitivity plot after lamination, after plasma treatment.

5.5.2.4.2 Hysteresis and Sensitivity study part II

a. Testing solution

I. Buffer: pH 5,6,7,8

II. Artificial sweat: pH 5,6,7,8

b. Conditions

I. Before lamination, before plasma treatment

II. After lamination, before Plasma treatment

III. After lamination, after Plasma treatment

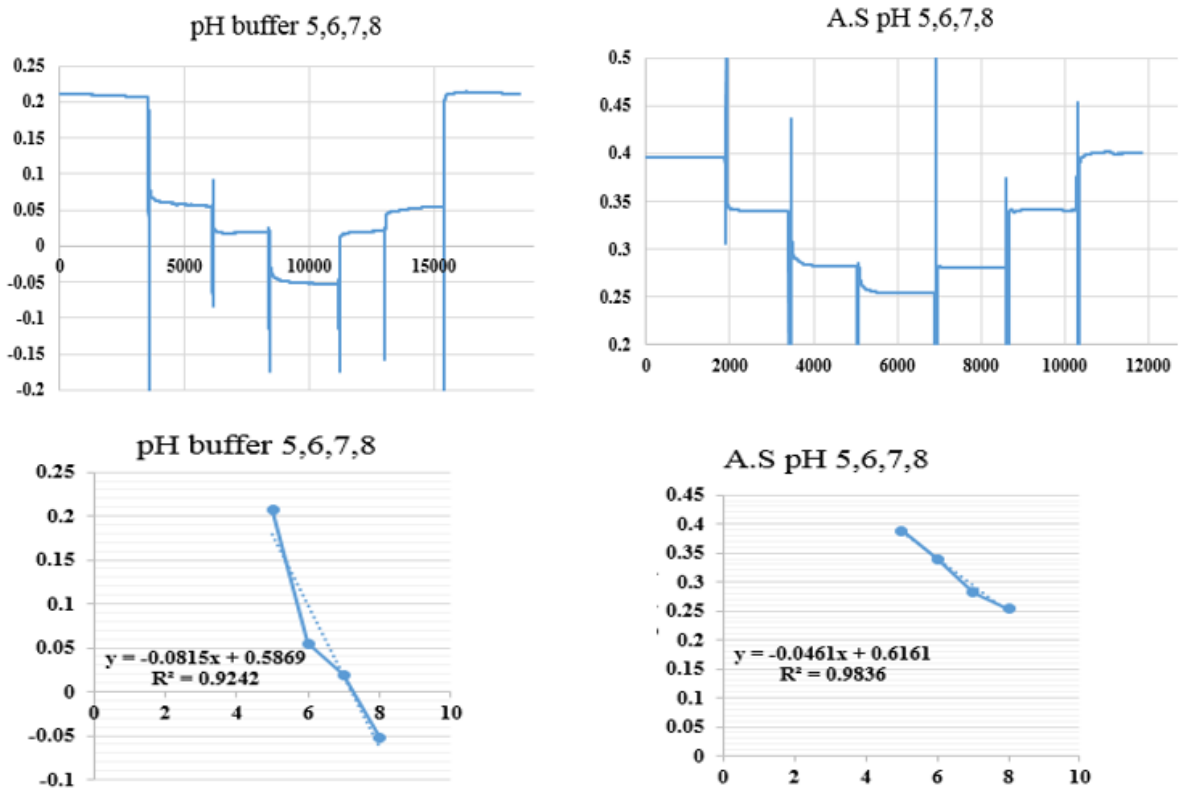

Fig 63 – Buffer and A.S at pH 5,6,7 and 8 under condition one

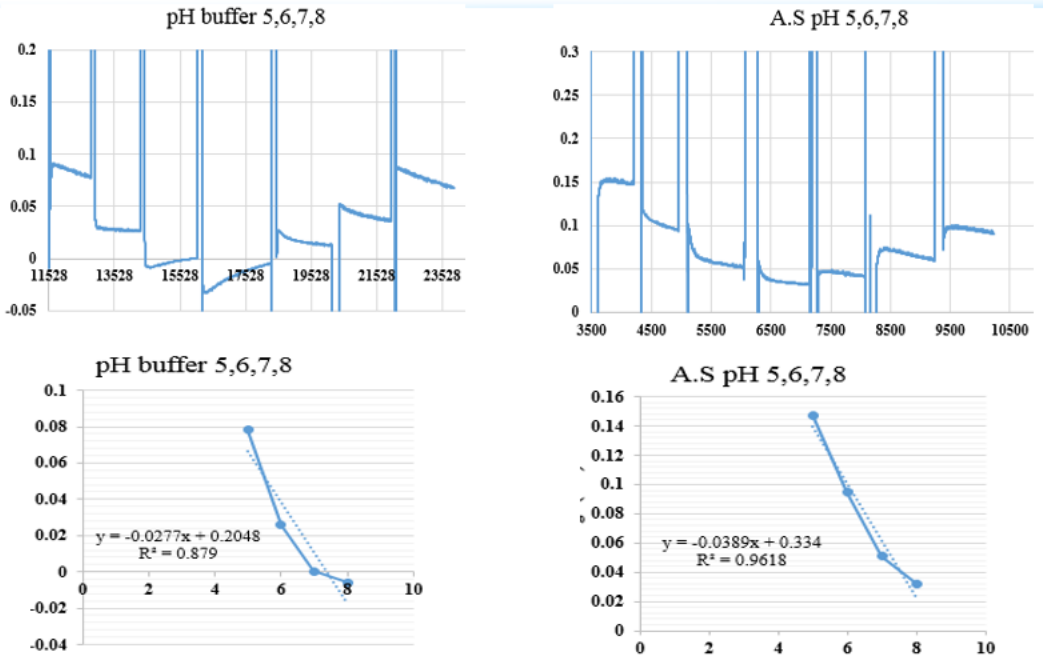

Fig 64 – Buffer and A.S at pH 5,6,7 and 8 under condition two

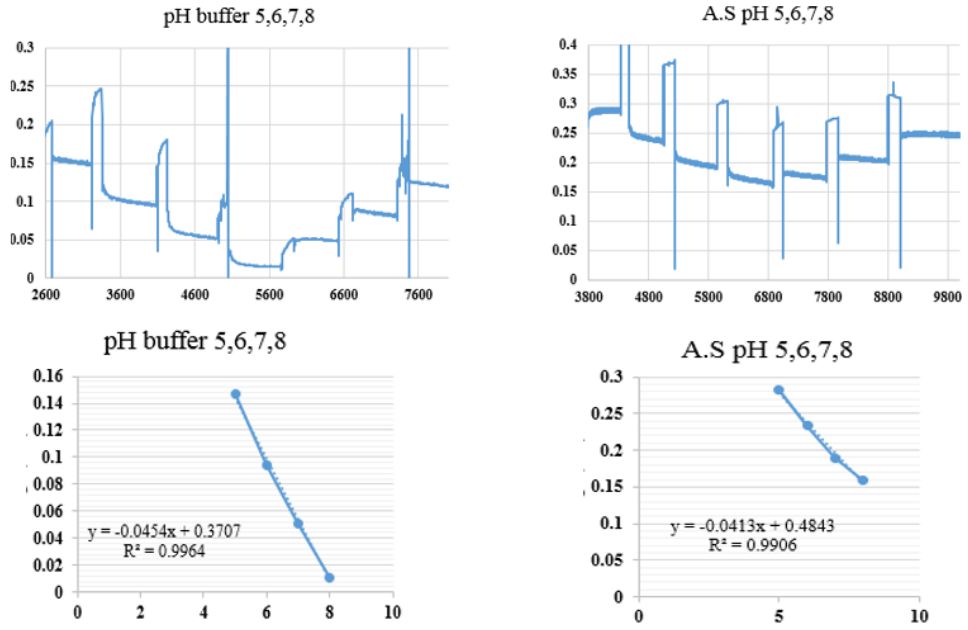

Fig 65 – Buffer and A.S at pH 5,6,7 and 8 under condition three.

From hysteresis and sensitivity study in part I and part II, it is observed that, pH electrodes after lamination suffer from severe hysteresis. Such behavior is supposedly due to reservoir situation created by laminating pouch, thereby effecting ionic interaction.

5.3.2.5 Troubleshoot

Proper functionality of an electrode is an important factor for good performance. Analyzing the hysteresis plot in figure 60 and 63, functionality of the electrode is proper.

Besides trying other alternatives such as using ultra flexible substrate, clean electrodes in DI water and in the presence of plasma, the hysteresis effect could not be eliminated. Changing the electrode design showed an improvement in response time but hysteresis effect could not be improved.

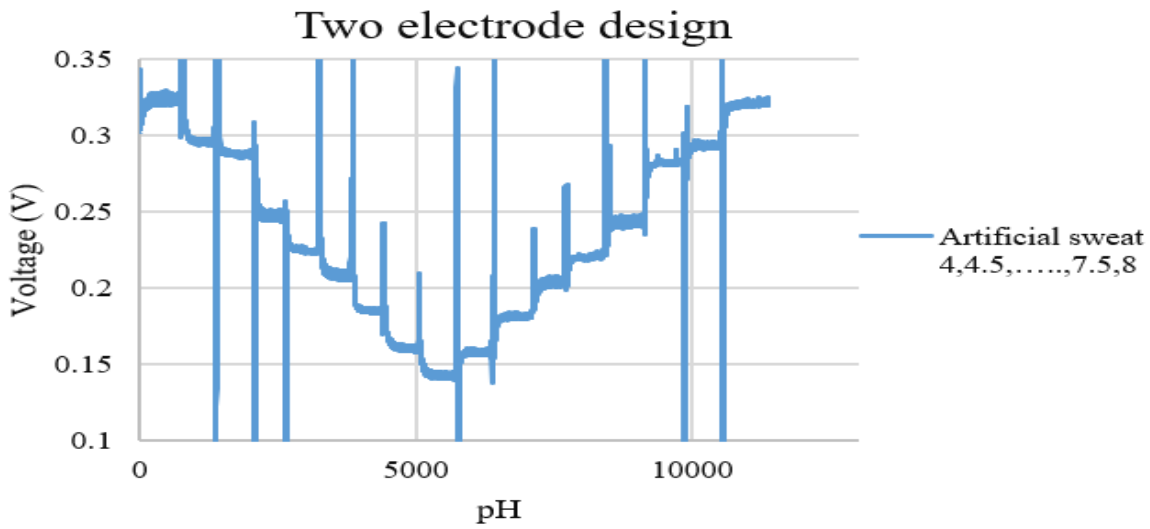

Figure 66 – Two electrode design

Before working on the array design with five electrodes, I started with two electrode design with one pH working electrode and one reference electrode. The two electrodes were laminated and tested in artificial sweat within the pH range of 4 to 8. Analyzing the hysteresis plot of two

electrode design, there is no convincing reason that reservoir effect created by thickness of the laminating pouch contributed to hysteresis effect in array design.

In the array design, there is no convincing reason to claim that factors like crosstalk between electrodes, reservoir effect and electrode functionality contributes to the hysteresis effect.

However, factors like thermal effect and viscosity are likely responsible for hysteresis problem in the array design. Double tape layered on the electrode is used to create insulation between the sensing window and other area of the electrode. When the sample passes through the laminator, under high temperature, thermal properties of the double tape and Iridium Oxide sensing film can change. The thermal reaction between the film and tape could have increased the impedance of the electrode thereby effecting the hysteresis performance. The thermal effects could not be observed under Scanning Electron Microscopy (SEM) because the sample is transparent in color. Viscosity of the artificial sweat could have changed over time. Few days after balancing the artificial sweat solution using hydrochloric acid (HCl) and sodium hydroxide (NaOH), the sample with two electrode design was tested. The array design was tested only weeks after the solution was prepared. Hysteresis study of two electrode design in figure 69 is not a concern but the hysteresis effect in the array design is severe.

Materials used for lamination were commercially available materials and their properties could not be changed. Due to time constraint, a cost-effective way of eliminating hysteresis could not be developed. To eliminate hysteresis problem, using photolithography and patterning the array is an option but it is not cost effective. Dash group also reports wearable device which is multifunctional.

Chapter 6

pH VALUE DISPLAY

6.1 Material and tools

All electrodes developed are based on Iridium Oxide sensing film, commonly known for its wide pH sensing range. Read out parameter is voltage, and voltage difference between the working and reference electrode decreases with increase in pH level of test solution. Real time voltage generated in high alkaline solution is very low, and the NI DAQ card reads them in negative values. Analog to digital converter (ADC) in the ATmega432P (Arduino) cannot read values in negative. So, we chose to use a differential amplifier circuit to transmit amplified signal to Arduino. ATmega432P is an 8-bit microcontroller, low power consumption tool, and operates between a voltage range from +1.8V to +5.5V. Arduino reads the amplified information and converts the data back to pH value and displays it on a screen.

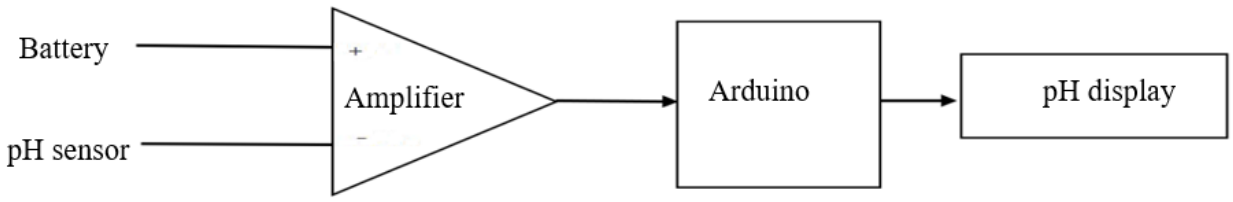

Fig 67- Tools used for pH value display

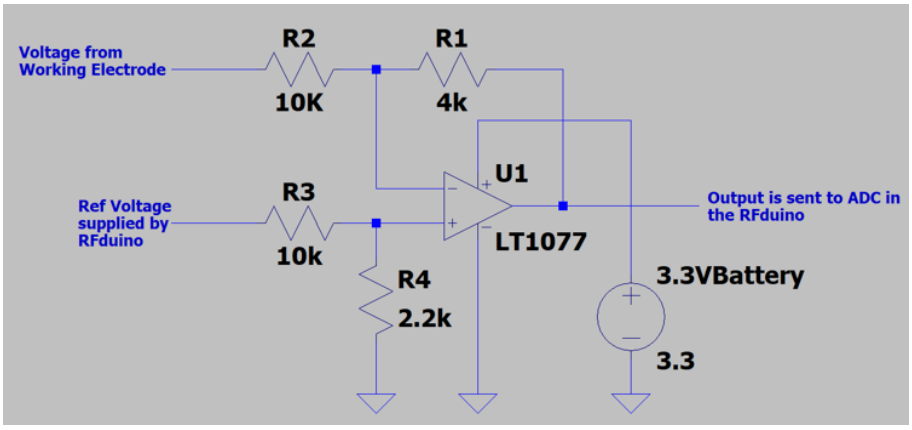

Fig 68- Differential amplifier circuit

In a pH scale of 1 to 14, Iridium Oxide based sensors generates bipolar signal. Read out parameter is in voltage, varies between 414 mV to -414 mV. Arduino cannot process data in negative range, which is why battery is used to upscale the voltage range. Amplifier is used to correct the input bias current. pH electrode is a high impedance electrode, small bias current creates a large voltage error. So, amplifier is used to reduce the biasing problem, and it transmits the amplified data to Arduino. Arduino converts the voltage to pH value and through graphical user interface (GUI) displays the value on a digital screen. Graphical user interface allows interaction between electronic devices and user, through graphical icons.

6.2 pH display value on digital screen

To read the pH value, slope and offset value can be found by plotting pH versus voltage graph in any spreadsheet system, for convenience Microsoft Excel is a good choice. A graphical user interface (GUI) is a type of user interface that allows interfacing between electronics and software icons. Programming language closely related to java is programmed on Arduino, and using GUI is used to display real time pH value on digital screen.

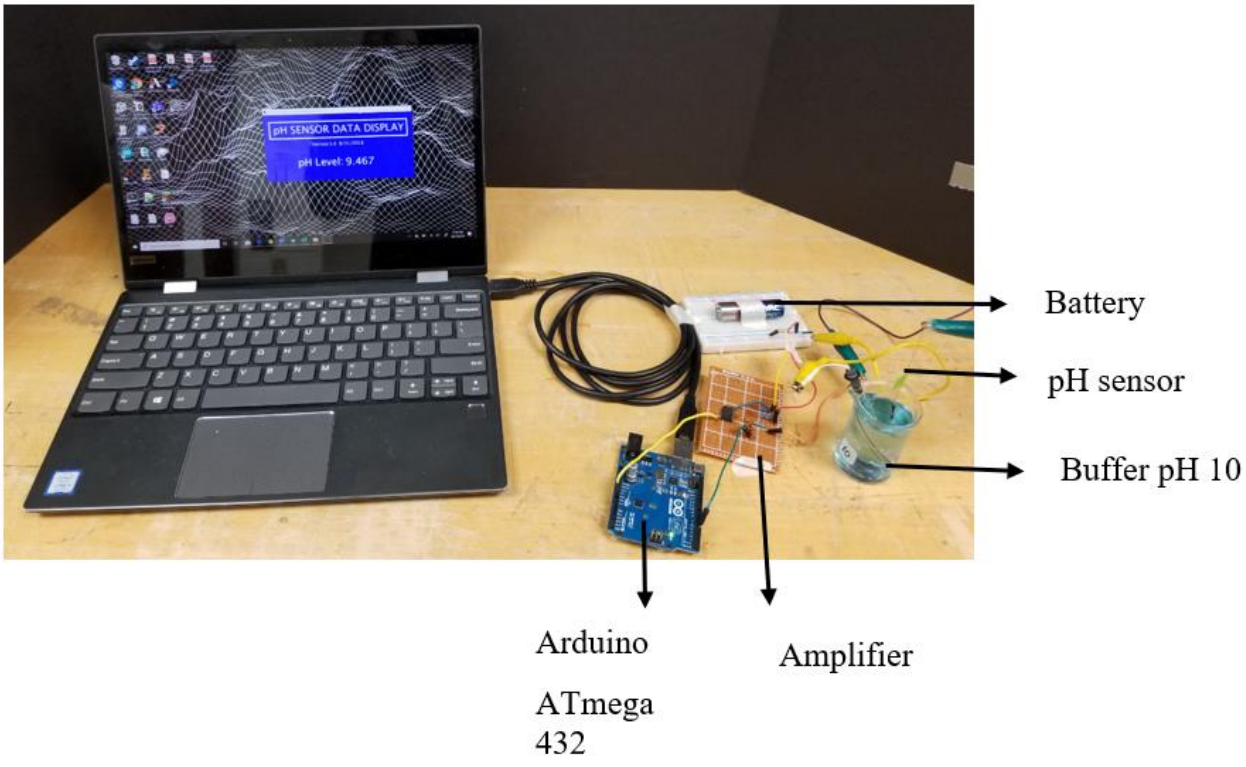

Fig 69-Real time pH value display

6.3 Concept for wireless pH sensing

Wireless pH sensing can also be developed by using two Bluetooth version RFduino (microcontroller atmega328p); part A acts as the transmitter and part B acts as receiver. The voltage generated between the working and reference electrode is amplified by the differential amplifier. Real time amplified voltage is then read by transmitter (part A), voltage is changed to pH value using the slope and offset value entered in the program, and the information is sent to the receiver (part B). Through GUI part B displays pH value on digital screen.

Reference

[1] J. Heikenfled, A. Jajack, B. Feldman, S. W. Granger, S. Gaitonde, G. Begtrup, and B.A. Katchman, “Accessing Analytes in Biofluids for Peripheral Biochemical Monitoring,” Nature, Vol. 37, pg. 407-419, 2019.

[2] O. Korostynska, K. Arshak, E. Gill, and A. Arshak, “Review Paper: Materials and Techniques for In Vivo pH Monitoring,” Sensors, Vol. 8, No.1, pg. 20-28, 2007.

[3] W. Huang, H. Cao, S. Deb, M. Chiao and J.C. Chiao, “A Flexible pH Sensor based on the Iridium Oxide Sensing Film,” Sensors and Actuators, Vol. 169, No. 1, pg. 1-11, 2011.

[4] P. Marsh, W. Moore, M. Clucas, L. Huynh, K. Kim, S. Y, H. Cao, J.C. Chiao, “Chracterization of Flexible pH micro-Sensors based on Electrodeposited IrOx Thin film,” Sensors, 2017 IEEE, 2017, Yamaka solution

[5] C. M. Nguyen, S. Rao, X. Yang, S. Dubey, J. Mays, H. Cao and J. C. Chiao, “Sol-Gel Deposition of Iridium Oxide for Biomedical Micro-Devices,” Sensors, Vol. 15, pg. 4214 – 4228, 2015.

Bibliographical Information

Khengdauliu Chawang received her bachelor's degree in Electronics and Communication Engineering from National Institute of Technology, Nagaland, India in July 2016. For senior year project, she worked on photodetectors and participated in poster presentation at ICETNMST, 2017. In Fall 2017, she enrolled at the University of Texas at Arlington (UTA) to earn Master of Science degree in Electrical Engineering. Keen on research, she joined the iMEMS group to work on her thesis in 2018 and served as a Graduate Research Assistant during the master's program. Her current work focuses on biomedical sensors, device fabrication and product design. And her research interest involves circuit designing, micro or nano fabrication, and MEMS devices.